Article:
Das, C, Read, DJ, Soulages, JM et al. (2017) Static and dynamic scaling close to gelation in chain-polymerization: Effect of reactor type. Macromolecular Theory and Simulations, 26 (3). 1700006. ISSN: 1022-1344

https://doi.org/10.1002/mats.201700006

DOI: 10.1002/marc.((insert number))

Article Type (Full Paper)

Static and dynamic scaling close to gelation in chain-polymerization: Effect of reactor type

Chinmay Das*, Daniel J. Read*, Johannes M. Soulages, Pradeep P. Shirodkar

---

Dr. Chinmay Das
School of Mathematics
University of Leeds,
Leeds LS2 9JT, United Kingdom
E-mail: c.das@leeds.ac.uk

Dr. Daniel J. Read
School of Mathematics
University of Leeds,
Leeds LS2 9JT, United Kingdom
E-mail: d.j.read@leeds.ac.uk

Dr. Johannes M. Soulages
Corporate Strategic Research
ExxonMobil Research and Engineering Company
Annandale, NJ 08801, USA

Dr. Pradeep P. Shirodkar
Global Chemical Research
ExxonMobil Chemical
Baytown, TX 77520, USA

Because of the familiarity of gelation theories in polycondensation reaction of multifunctional groups, often the gel-point is defined as the point of diverging weight averaged molar mass. We present an industrially-relevant counter-example to this common perception. Chain-growth polymerization in realistic reactors introduces history dependent crosslinking probability. For copolymerization of a two functional monomer (ethylene) with a four functional comonomer (non-conjugated diene), we show from a Monte Carlo scheme that standard gelation scaling exponents remain valid for a semibatch reactor. However, for syntheses in a continuous stirred

tank reactor (CSTR), all commonly measured molar mass moments (number, weight and `z'-averaged moment) remain finite at the gel-point; the first moment to diverge is the fourth moment. Hence, identification of the gel point from experimental observations is difficult, and cannot be achieved through monitoring of the weight averaged molar mass. We use a numerical scheme based on the tube model of polymer melts to predict the rheology of the generated molecules. Stress relaxation follows a power-law decay, but due to dynamic dilution effects the CSTR resins exhibit much slower increase in the zero shear viscosity as the gel point is approached as compared to the semibatch reactor resins.

1. Introduction

In many branched polymer synthesis, certain reaction conditions lead to gelation with diverging molar mass of the largest molecule (network formation). Since the seminal analysis of Flory[1] and Stockmayer,[2] step-growth polymerization (or polycondensation reaction)[3] served as the archetypal example of this sol-gel transition in polymer synthesis. During polycondensation reaction involving monomers with functionality $f \geq 3$, the molar mass of the largest molecule diverges as the reaction probability p of the functional groups reaches a certain critical value p_c. Close to the gel point, the resins exhibit universal features in both the static properties[1,2,4] (high molar mass tail of the molar mass distribution follows a power-law with a universal exponent, the weight averaged molar mass diverges as a power of normalized distance to the critical probability) and in dynamics[5,6] (relaxation follows a power-law in time, incorporating self-similar distribution of modes). The success and simplicity of the statistical description of gelation in polycondensation has often led to usage of the same results in other polymerization processes, often without any real justification.

In classical models of gelation via a polycondensation reaction,[1,2,7,8] one usually considers equal probability of reaction for each of the functional groups. Similarly, in vulcanization one considers equal probability of crosslinking of preexisting chains. This assumption of equal probability of crosslinking fails when one considers realistic reactors. In chain growth polymerization (or, addition polymerization)[3] unsaturated monomers add onto the active site of a growing chain one at a time. In many synthesis processes, polymerization and crosslinking occur in the same reactor: a monomer with multiple terminal unsaturated bonds first gets incorporated in a growing chain. At a later time, another terminal unsaturated bond of the same monomer can be incorporated in another growing chain leading to branching. As we show below, the probability of such branching becomes dependent on the details of the reaction

history of this particular monomer. Different multifunctional monomers acquire different crosslinking probability because of the different available times for the second reaction to happen in the reactor. So far, a systematic study looking at the scaling properties in chain growth polymerization as the gel point is approached has received little attention, mainly limited to free-radical polymerization;[9–12] often with the *a priori* assumption that the gel point is defined by divergence of the weight-averaged molar mass.

In this paper, we consider copolymerization of a bi and a tetra functional monomers (phrased in terms of ethylene and non-conjugated diene) with a metal catalyst in realistic reactor conditions: in a semibatch reactor and in a continuous stirred tank reactor (CSTR).[13] Comparing with polycondensation reactions, the ethylene monomer is equivalent to a bifunctional polycondensation monomer in the sense that its incorporation into a growing polymer gives rise to locally linear chain sections. In contrast, the diene comonomer is equivalent to a four-functional polycondensation monomer in that, when all groups are reacted, a branchpoint is formed linking four linear chain sections at their ends. In a batch reactor, all reactants are placed in the reactor at the start of the reaction. In a semibatch reactor, some of the gaseous monomer types are replenished by maintaining a constant gas pressure during the reaction. In the CSTR, all reactants are introduced in the reactor at a constant rate and product resin is removed continuously. We assume ideal mixing for both reactors here. A small amount of long-chain branching (LCB) can drastically alter the flow properties of polymer molecules[14–16] and is often exploited for better processability when shear thinning or extension hardening at low rates are desired. In the past few decades, constrained geometry metal catalysts,[17] like metallocenes, have allowed synthesis of polyolefin resins of well-defined structure and comparatively narrow polydispersity. Under certain reaction conditions, vinyl terminated segments (macromonomers) can be incorporated in another chain growing at a later time[18] forming three-functional branches. However, the density of such macromonomer-induced branches is typically small. Non-conjugated dienes (small molecules, often short linear alkenes,

with two terminal double bonds at each end) can be used to increase the amount of branching in polyolefin resins.[19,20] Contrary to the single terminal double bond in a macromonomer, copolymerization with diene introduces pendant double bonds at each of the incorporated diene sites. Thus copolymerization with diene provides a route to create much more branched resins than is possible in homopolymerization of olefins.

Understanding and eventually predicting the molecular structures created during this copolymerization can help in optimizing reactor conditions for desired flow properties of the manufactured resin.[16] Equally importantly, such a knowledge would help in avoiding reactor fouling (while often high level of branching is preferred, reaching post-gel conditions in the reactor results in reactor downtime and costly cleanups[21,22]). Because of its commercial relevance, ethylene-diene copolymerization (often considered along with another comonomer like hexene, octene or propylene to control crystallinity by introducing short-chain branches[23]) has been the focus of a number of patents[24–28] and publications.[20,29–31] However, the theoretical modeling of this important class of polymerization[32–35] has been mostly limited to calculations based on the method of moments. In this methodology, the branch-formation step couples the equations relating different moments. The set of infinite equations is reduced to a smaller set of equations (often just two), by introducing a closure hypothesis for higher moments, or by assuming some particular form of chain length distribution beyond a certain molar mass. The gel point is identified by considering either the divergence of the weight-averaged molar mass,[34] or the non-existence of any real root for the weight averaged molar mass[32] from the closed equations with untested closure hypothesis. In general, the divergence of molar mass of the largest polymer does not ensure concomitant divergence of the second moment of the molar mass distribution. Close to gelation, the number distribution of molecules scales as a power-law of molar mass with some exponent τ. The second moment of the molar mass distribution at gelation is the first moment to diverge only for $2 < \tau \leq 3$. For polycondensation reaction, τ satisfies this inequality. But as we show in this paper, this is not

the case for all polymerization schemes. Another possible route for calculating the molar mass distribution is direct numerical solution for the "population balance" of different species in the reactor (e.g. using finite element methods[36]). We expect that this method, properly applied, would result in similar conclusions to ours. However, for the particular set of reactions considered in this work, the balance equations would need to track the concentration of species varying with respect to five separate variables (degree of polymerization, number of branches of two different types, number of unsaturated groups of two different types), paying close attention to the tails of the distribution for each variable. We believe that under such circumstances our Monte Carlo approach detailed below is a competitive method, despite the care needed in obtaining a statistically significant number of large molecules.

A route to gain detailed information about the structure of the molecules, which does not suffer from the closure problem of moment-based calculations, is a stochastic simulation of the polymerization process. Two quite distinct stochastic approaches have been developed for generating polymers from a certain reaction scheme. The first, direct stochastic simulation of the rate equations,[37] remains computationally costly with much of the computational cost being used in creating a library of branched structures that would be present in steady state. The second, stochastic Monte Carlo sampling at the segment level,[11,38] starts with calculations of the probabilities for different branching scenarios. Armed with the probabilities of various branching events, one can avoid the necessity of having a library of shapes and can generate representative in silico molecules one at a time. By generating a large ensemble of molecules for given reaction conditions, one can calculate both the structural and flow properties.

In the following section (Section 2), we start by introducing such a segment level Monte Carlo scheme for ethylene-diene copolymerization with a metallocene catalyst. Next we use the Monte Carlo scheme in Section 3 to generate numerical ensembles of molecules and probe the static properties of the resins as gelation is approached with increasing diene concentration. The

sol-gel transition can be viewed as a geometric phase transition and has been modeled as a percolation transition on a lattice.[39,40] In the simplest form of the bond-percolation model,[39] one considers a regular lattice (for example, a cubic lattice) with bonds forming between adjacent lattice points with some fixed probability p. The size of the largest connected cluster diverges at a critical value of probability p_c and the various measurable quantities scale as power-laws close to p_c with exponents that are independent of the details of the underlying lattice. The mean-field description of the classical gelation model[1,2] can be viewed as a percolation on a Bethe lattice (Cayley tree) and, hence, neglects loop formation. During polymerization under usual conditions, except in a narrow window that decreases with the segment length between branchpoints,[41] the influence of loops can be neglected and the exponents are expected to be mean-field-like. Polycondensation of tri-functional oligomers of increasing length has been used to experimentally observe the exponents changing from the percolation-like to mean-field-like values.[42]

Our modeling neglects loop-formation and hence, at a first glance, is expected to give classical mean-field exponents. However, percolation models (either critical percolation on a regular lattice or mean-field gelation on a Bethe lattice) typically assumes a fixed probability of bond-formation. This is an appropriate choice for vulcanization, but not for realistic reactors considered in this work. With a fixed rate of incorporation of a pendant diene, a polymer segment that is created just before the reaction ended has effectively zero probability for cross-linking at the incorporated pendant diene sites. Similarly, a polymer segment that survives in the reactor for very long times will have all the pendant dienes eventually incorporated in another growing segment. For the parameter space explored in this work, we find that the exponents for the divergence of the static structures remain classical mean-field-like in the semibatch reactor with the weight averaged molar mass diverging as gel-point is approached. Changing the parameters only affects the critical amplitudes without modifying the exponents. The divergence of the molar mass in the CSTR case is dominated by a very small population

of molecules that remain in the reactor for longer than average duration. All commonly measured low-order moments of molar mass are found to remain finite at the gel-point with the 4-th moment of the molar mass being the first moment to diverge. Associated with these finite lower-order moments are exponents that are different from the classical mean-field model for gelation. Unlike the semibatch case, the exponent describing the power-law region of the molar mass distribution reaches a constant value only very close to the gel-point.

Close to gelation, the shear relaxation modulus decays as a power-law in time.[5,6] The dynamical exponents are not universal and cannot be calculated without additional assumptions about the relaxation dynamics. In Section 4 we use the numerical ensembles of molecules generated from our Monte Carlo simulations to calculate the rheological responses in the melt state using a numerical scheme[43] based on the tube theory of entangled polymers.[44] As the gel point is approached for resins from either of the reactors, the shear relaxation moduli were found to decay as power-law in time (over suitable time range that increases with proximity to the gel point) with very similar exponents. However, the zero shear viscosity or the recoverable compliance for resins synthesized in CSTR shows much gentler increase as the gel-point is approached when compared to the resins synthesized in semibatch reactor.

We end this paper (Section 5) with a detailed discussion on the relevance of our modeling to experimental synthesis of ethylene-diene copolymers, and to other chain-growth polymerization processes.

2. Monte Carlo scheme

2.1. Reaction Kinetics

We consider a set of reaction steps that has been used to describe polymerization of polyolefins with metallocene catalysts,[18] supplemented by reaction steps involving non-conjugated

diene.[45] Schematically the reaction steps are shown in **Figure 1**. An activated catalyst binds to a monomer to initiate polymerization. Ethylene and unreacted diene are incorporated with respective rate constants k_p and k_{pD} . The catalyst detaches itself from the growing chain leaving behind a double bond with rate $k_=$ or a saturated chain end with rate k_s. Molecules having terminal double bond, macromonomers ($P^=$), are incorporated in a growing chain with rate constant k_{PLCB}. Irrespective of the presence or absence of the terminal double bond, molecules can be incorporated in a growing chain with rate constant k_{DLCB} at the point where a once reacted diene leaves a pendant double bond. For semibatch reactor, we assume that the catalyst is deactivated at a rate k_d during termination events without assigning any particular mechanism behind this deactivation process.

2.2. Monte Carlo sampling

We consider the population balance equations implied by the rate equations and analytically compute the concentrations of the various species and the probabilities of branch formation. Starting from a randomly chosen reacted monomer in the final product, we use these probabilities to recreate a probable life history of a single molecule. Repeating this a (potentially large) number of times, we generate an ensemble of molecules that collectively follows the analytically determined probabilities of branching.

We consider a well-mixed CSTR reactor at steady state or a well-mixed semibatch reactor with monomer being continuously replenished. For the semibatch reactor, the monomer concentration $[M]$ remains fixed, but the concentration of active catalyst $[Y](t)$ and that of unreacted diene $[D](t)$ decreases with time. For this case, it is convenient to consider the monomer conversion x (concentration of reacted monomer $[M_R]$ normalized by the equilibrium monomer concentration $[M]$) as the proxy for time. Note that the monomer conversion defined in this way can be larger than unity. The monomer conversion x and the time t are related by

$$x = \frac{k_p[Y]_0}{k_d}\,[1 - \,e^{-k_d t}]. \qquad (1)$$

Here, $[Y]_0$ is the initial catalyst concentration. We denote the final monomer conversion in the semibatch reactor by x_f and the corresponding time of reaction by t_f.

Once a free diene is incorporated in a growing chain, there is a pendant double bond created. We denote the density of such pendant double bond from once-incorporated diene as $[D_1]$. Concentrating on a particular growing chain, we will distinguish between two different kind of diene-induced long-chain branching: (i) the growing chain can incorporate a free diene creating a pendant diene. The pendant diene is incorporated in another chain growing at a later time. We denote this branching event as of type b_{D1}. (ii) the growing chain can incorporate a pendant diene that is already part of another chain grown in the past. We denote this branching event as of type b_{D2}. Chains ending with a terminal double bond can be incorporated in another growing chain at a later time. We term this branching from macromonomer as of type b_m.

The derivation of the Monte Carlo scheme follows closely existing studies[11,38,45] for other polymerization scenarios and we only present an outline of the algorithm in the appendix.

2.3 Simulations

For our numerical explorations, we choose $[M] = 0.3$ mol/L, $k_p = 500$ L/mol-s, $k_{pD} = 30$ L/mol-s, $k_= = 0.2$ /s, $k_s = 0.005$ /s, $k_{PLCB} = 1$ L/mol-s, and $k_{DLCB} = 0.2$ L/mol-s. The monomer molar mass is chosen to be 28 g/mol corresponding to that of ethylene. Because the relative concentration of incorporated diene remains very small even at gelation, we neglect the molar mass contribution from diene. For the CSTR calculations, we explicitly consider an active catalyst concentration of $[Y] = 10^{-3}$ mol/L. For the semibatch reactor, we consider a catalyst deactivation rate $k_d = 10^{-3}$ /s. While the orders of magnitude of these parameters correspond to some previous modeling of experimental resins with metallocene catalysts,[46] the individual values of the parameters are probably not so relevant. Only a small number of

nontrivial combinations of these parameters determine the long-chain branched structure of the molecules.[47] For both the CSTR and the semibatch reactor, we vary $[D]$ starting from a small concentration (10^{-6} mol/L) until the point we can no longer reliably estimate the moments of the molar mass or until the level of recursion reaches a predetermined value (see below). For the CSTR case, we consider a number of different mean residence times (τ_{res}). Similarly, for the semibatch reactor, we consider a number of different final conversions.

With increasing diene concentration, some of the molecules can become highly branched with many segments. Equivalently, our recursive algorithm can reach many levels of recursion, eventually exceeding the available stack size. For a particular parameter set, if the level of recursion reaches more than 260 during generation of a molecule, we reject the molecule. If two such rejections are found while generating 10^6 molecules, we consider numerically being close enough to the gel-point and do not proceed any further in increasing the diene concentration. The maximum recursion level of 260 is arbitrarily fixed from the observation that for recursion levels slightly more than this, the memory requirement becomes larger than that is available (2GB) for the particular computer in which simulations were performed. For the semibatch reactor, this exhaustion of available stack is the limiting resource that determines how close we can approach the gel-point.

For each values of $[D]$, we calculate the first five moments of the molar mass by considering 10^6 molecules (the choice of the first five moments was from some exploratory simulations that suggested that for the CSTR reactor, the divergences of the fourth and the fifth moments occur at the same diene concentration with the lower moments remaining finite at that concentration). From 9 separate such simulations, we calculate the error estimates on the molar mass moments. If the relative error in the fourth moment was found to be larger than 1%, we generate another 9×10^6 molecules and recalculate the averages and error estimates using all the additional molecules generated. We continue this process of increasing the generated number of molecules

until we either reach error estimates within our chosen criteria or the number of molecules generated becomes larger than 10^9 . This provides a second criterion for how close to the gel-point we can go numerically: If with 10^9 molecules we cannot estimate the fourth moment within 1% relative error, then we discard the simulation. For the CSTR case, this lack of convergence of higher moments decides how close we can approach the gel-point.

Using the highest calculated decade in diene concentration, we use the nonlinear Levenberg-Marquardt algorithm[48] to fit the molar mass moments in a power-law form. The initial values for the critical diene concentrations were set from a linear extrapolation to zero value of the inverse of the moment and the initial values of the amplitudes were set to the value of the molar mass moment at low diene concentration.

For the CSTR case, we also separately considered catalysts that do not allow macromonomer incorporation (i.e. k_{PLCB} was set to zero with all other rate constants kept the same).

For a single value of conversion in semibatch reactor and a single residence time in CSTR, we use the generated molecules at various diene concentrations to calculate the rheological responses and investigate the dynamical scaling close to gelation.

3. Scaling of molar mass distributions

Concentrating on the pre-gel conditions, we define the closeness to the gel-point as[4]

$$\varepsilon = \frac{[D]_C - [D]}{[D]_C}, \tag{2}$$

with $[D]_C$ being the critical concentration of diene at which the characteristic molar mass (defined below via Equation 3) diverges. Close to $[D]_C$, the *number* distribution of polymers of molar mass M is expected to scale as[4]

$$\phi_N(M) \sim M^{-\tau} f\left(\frac{M}{M_{char}}\right), \quad (3)$$

with an exponent τ. The cut-off function f is a function which is equal to 1 for $M \ll M_{char}$ and which decays rapidly for $M > M_{char}$ so that M_{char} is a characteristic molar mass above which the power-law scaling is suppressed. As gelation is approached, M_{char} diverges with an exponent 1/σ as

$$M_{char} \sim \varepsilon^{-1/\sigma}. \quad (4)$$

The moments of molar mass

$$M_k \equiv \frac{\int \phi_N(M)\, M^k\, dM}{\int \phi_N(M)\, M^{k-1}\, dM}, \quad (5)$$

diverge for all $k \geq \tau - 1$ as powers (or logarithmically when $k = \tau - 1$) of M_{char} and hence as powers of ε from Equation 4.

In both lattice-percolation ($\tau \approx 2.2$ in 3-dimensions) and mean-field gelation models (τ = 5/2), the first (integer) moment to diverge is the weight averaged molar mass $M_2 \equiv M_W$, defining another exponent γ

$$M_W \sim \varepsilon^{-\gamma}. \quad (6)$$

Keeping the possibility open that the first moment to diverge may not be the second one, we define a more general version of this power-law dependence as

$$M_k \sim \varepsilon^{-\gamma_k}. \quad (7)$$

In trying to estimate the exponents, we first calculate different moments M_k for $k \leq 5$ as a function of $[D]$.

We emphasize here that the gel point is correctly defined as the point where M_{char} diverges, irrespective of the exponent τ. Other works on branched polymer formation in CSTR[12,49] have noted a variation in an apparent exponent τ with reactor variables and have (erroneously)

defined gelation as the point where τ decreases past a value of 3. This, of course, is the value of τ below which the weight averaged molar mass diverges, but it does not define the gel point.

3.1 Semibatch reactor

For the semibatch reactor, **Figure 2**(a) shows the number distribution of molar mass for $x_f = 50$ ($t_f \approx 105$ s) and $[D]_0 \equiv [D](t = 0) = 0.294$ mol/L. The high molar mass end of the data can be described well over three decades with a power-law dependence and an exponential cut-off function characteristic of mean-field theory[4]. The exponent $\tau = 2.492(2)$ from the fit in Figure 2 is close to the mean-field prediction of 5/2.

Figure 2(b) shows the weight averaged molar mass M_W as a function of initial diene concentration. The fit gives an exponent $\gamma = 1.005(8)$ for the scaling of M_W that is consistent with the mean-field prediction of 1. The fit also provides estimate of the critical diene concentration at which M_W diverges as $[D]_c$= 0.3095(2). Repeating the fitting exercise with the number averaged molar mass M_N (first moment of the molar mass distribution) gives an apparent critical concentration $[D]_c$=1.04(2), showing that M_N remains finite as the gel-point is approached. For moments higher than 2, the fitting retrieves the same critical diene concentration as with M_W. In particular, fitting of third moment M_Z predicts $[D]_c$= 0.3097(2).

From fitting the molar mass distribution with mean-field exponential cut-off (Figure 2), we calculated M_{char} for different values of $[D]_0$ and hence for different ε. **Figure 3**(a) shows the plot of M_{char} as a function of ε. The fit gives 1/σ = 2.06(2), a value close to the mean-field prediction of 2.

From a series of simulations at different final conversions, we calculated the critical diene concentration required for gelation at each of these final conversions. Increasing the time of reaction leads to gelation at lower initial diene concentrations (Figure 3b). A physically more meaningful quantity is the average number of diene links per primary segment (defined as the

segment generated from initiation until termination) at gelation threshold. To calculate the number of links per primary segment, we start with the concentration of twice reacted diene at a certain conversion x

$$[D_2](x) = [D]_0 \frac{k_{pD}k_{DLCB}}{k_{DLCB} - k_{pD}} \left[\frac{1 - \exp(-\frac{k_{pD}}{k_p}x)}{k_{pD}} - \frac{1 - \exp(-\frac{k_{DLCB}}{k_p}x)}{k_{DLCB}} \right]. \quad (8)$$

The ratio of $[D_2]$ and $[M]x_f$ evaluated at x_f gives the number of diene link per reacted monomer. In order to find the average number of links per primary segment at the gel point, we set $[D]_0$ as the critical value extrapolated from scaling of M_W and multiply by the degree of polymerization of a primary segment $\equiv k_p[M]/(k_= + k_s)$. **Figure 4** shows that at small conversions, the number of links per primary segment approaches the simple estimate 1/2 as expected for vulcanization of linear polymers. In semibatch reactor, for short reaction times, the macromonomer incorporation plays no role (their density is effectively zero). With increasing reaction time, the presence of three functional macromonomer induced branching reduces the number of diene induced four functional links required to reach gelation. The inset of Figure 4 shows the mole fraction of diene to that of monomer in the resins at gelation, estimated as $[D]_c\big(1 - \exp(-k_{pD}x_f)\big)/\big([M]x_f\big)$. For short reaction times, most of the incorporated dienes remain as pendant short chains and do not have the possibility of undergoing the second incorporation to produce a long-chain branch. At conversion $x_f = 200$ ($t_f \approx 521$ s), for the particular values of rate constants we have chosen in this work, diene occupies 0.002 mole fraction. Even at this high conversion, only about 7% of these incorporated diene contributes to branch-points.

3.2 Continuous stirred tank reactor

The approach to gelation in CSTR conditions turns out to be quite different from classical mean-field predictions for polycondensation reactions. First, we concentrate on $\tau_{res} = 100$ s. The

weight averaged molar mass can be fit to a power-law to find an apparent critical diene concentration $[D]_c$= 0.0373(1) mol/L (**Figure 5**). However, higher moments diverge before this concentration. **Figure 6** shows apparent $[D]_c$ calculated by fitting power-law divergence to the first five moments of the molar mass. In the figure, we denote the critical diene concentration estimated from the k-th moment as $[D]_{c,k}$. These estimates of $[D]_{c,k}$ suggest that the first moment to diverge is the fourth moment at $[D]_c$= 0.0237(3) mol/L. The inset of Figure 6 shows the ratios of apparent $[D]_c$ calculated by fitting a power-law to successive moments of the molar mass for a number of different τ_{res}. For $\tau_{res} = 100$ s, the critical diene concentration predicted from the power-law fit for M_Z is $\sim 15\%$ higher than that estimated from the power-law fit for M_4.

In **Figure 7**, we plot the number distributions for several different diene concentrations, and with $\tau_{res} = 100$ s. In calculating these distributions, we used 2×10^{10} molecules to resolve $\phi_N(M)$ reliably at the high molar mass. Even at the highest diene concentration considered, the data looks qualitatively different from the semibatch case (Figure 2). At high diene concentrations, two distinct power-law regions can be identified (indicated by dashed lines in Figure 7) with exponents that depend on $[D]$.

To accommodate two power-law features, we fit a functional form

$$\phi_N(M) = \frac{A}{M^{\tau_1}} \frac{1-exp\left(-\left[\frac{M}{M_X}\right]^{\tau-\tau_1}\right)}{\left[\frac{M}{M_X}\right]^{\tau-\tau_1}} \; exp\left(-\frac{M}{M_{char}}\right), \tag{9}$$

with a cross-over molar mass M_X. For $M < M_X$, $\phi_N(M)$ decreases as $M^{-\tau_1}$. For $M > M_X$, $\phi_N(M)$ decreases as $M^{-\tau}$ and eventually decreases exponentially beyond M_{char}. **Figure 8** shows the number distribution along with fit of the form in Equation 9 for $[D] = 0.022$ mol/L.

The variations of the exponents τ_1, τ and the molar masses M_X and M_{char} with the distance to the gel-point ε are shown in **Figure 9**. The cross-over molar mass M_X can be well-described for

small ε by a linear form: $M_X = 6.09(7) \times 10^5 - 5.21(2) \times 10^5\ \varepsilon$. The characteristic molar mass diverges as $\varepsilon^{-1.28(6)}$. Both the exponents τ_1 and τ vary with ε. A linear fit from the lowest four ε data gives the limiting $\tau_1 = 2.48(1)$ and $\tau = 4.48(2)$ at the gel-point. Since only the moments of molar mass with $k > \tau - 1$ diverges, this is consistent with our previous finding in Figure 6 that the first three molar mass moments remain finite at the gel-point.

We can qualitatively understand the long-tailed behavior of $\phi_N(M)$ by noting the exponential distribution in the residence time of individual molecules. Even in the absence of diene, a strand destined to remain for a long duration in the reactor has higher probability of being reincorporated in another growing strand. Since each of the primary strands are on average of the same length, molecules with longer than average residence times are typically more branched, resulting in higher molar mass from this macromonomer incorporation process. In the presence of diene, any pendant diene in a long-lived segment is almost certain of leading to a long-chain branch and hence to molecules with larger molar mass. To isolate the effect of diene, we have separately simulated the case where macromonomer incorporation is not allowed ($k_{PLCB} = 0$). This can be achieved experimentally by using a catalyst that has very low reactivity for macromonomers. **Figure 10** shows that even without macromonomer incorporation, the first moment of molar mass to diverge is the 4-th moment. Though in this case, the estimates of $[D]_c$ from the third moment is only about 5-10% higher than that from the fourth moment.

Figure 11 shows the estimated critical diene concentration (estimates from the 4-th moment of the molar mass) as a function of τ_{res} both with (open circles) and without (filled squares) macromonomer incorporation. For small τ_{res}, even when allowed, macromonomer incorporation induced branching has a low probability. Hence, the simulations predict the same $[D]_c$ irrespective of whether macromonomer incorporation is included or not. Since the probability of branch formation from incorporated diene increases with τ_{res}, in both cases $[D]_c$

decreases with τ_{res}. When macromonomer incorporation is allowed, molecules residing for a long duration in the reactor also acquire 3-functional branches. This lowers the $[D]_c$ significantly at large τ_{res} compared to the case where macromonomer incorporation is not allowed. The inset in Figure 11 shows the estimated number of 4-functional branches from diene per primary segment at gelation, estimated as $k_{DLCB}k_{pD}[Y][D]_c/\{(k_= + k_s)(k_{DLCB}[Y] + s)\}$. Without macromonomer insertion (solid symbols), the gel point is reached when the average number of 4-functional branches (H links) reaches about 0.1 per primary segment. When τ_{res} is large and macromonomer incorporation is allowed, the average number of diene branches required to reach gelation can be extremely small. For $\tau_{res} = 1000$ s and $k_{PLCB} = 1$ L/mol-s, only 0.014 diene induced branches per primary segment on average suffices to reach gelation.

Polymer resin molar mass distribution is often characterized by a single measure of average (typically weight averaged molar mass M_W) and a single measure of the width of the distribution (traditionally polydispersity index or PDI, defined as the ratio of M_W and M_N). When gelation is accompanied by diverging M_W, as in the semibatch reactor considered in this paper, the PDI also diverges at the gel point. By contrast, with diverging fourth moment at gelation, PDI remains finite in the CSTR case. **Figure 12** shows the PDI without diene and with the diene concentration set to the critical concentration $[D]_c$ (from extrapolation of M_W and M_N data obtained at lower diene concentrations). In the absence of diene, with increasing τ_{res}, the PDI with macromonomer incorporation (open squares) increases. In the absence of macromonomer incorporation, the PDI remains close to a value 2.0 in the absence of diene. At the gel-point, the PDI increases compared to the diene free case. In the inset of Figure 12, we show the ratio of the PDI at critical diene concentration normalized by the PDI at zero diene concentration. The relative increase in maximum PDI that can be achieved in the pre-gel state in the absence of

macromonomer incorporation is ≈ 2.5, when the residence time is large. With macromonomer incorporation, the relative growth in PDI is much lower.

4. Dynamic scaling

Close to gelation, the stress relaxation and rheological responses also follow scaling forms:[5,6,50] the shear stress relaxation function $G(t)$ behaves like a power-law in time (t)

$$G(t) \sim t^{-u}, \tag{10}$$

and the complex viscosity $\eta^*(\omega)$ follows a power-law in frequency (ω)

$$\eta^*(\omega) \sim \omega^{u-1}. \tag{11}$$

As the gel point is approached, the zero shear viscosity η_0 diverges as

$$\eta_0 \sim \varepsilon^{-s}, \tag{12}$$

and the recoverable compliance J_e^0 diverges as

$$J_e^0 \sim \varepsilon^{-t}. \tag{13}$$

To calculate the rheological properties of the polymers synthesized via our reaction scheme, we use a computational rheology software[43,51,52] developed by us. With only two main chemistry dependent parameter, viz. the entanglement molar mass M_e and the entanglement time τ_e, melt state flow properties of entangled polymers are well described by the 'tube theory'.[44,53] In a mean field sense, each polymer strand in the melt is confined in a tube-like potential due to the topological constraint of uncrossability of all the polymer molecules. Deformation is assumed to be affine down to the lengthscale of the tube diameter and relaxation proceeds hierarchically from outside in[54,55] as the molecules escape from the old deformed tube and attains equilibrium conformation. Because the tube potential in melt is due to the molecules themselves, the

potential softens (or equivalently the tube diameter increases) as relaxation proceeds.[56] This dynamic dilation couples the relaxation of all the molecules and necessitates numerical schemes[43,55,57] for a polydisperse (both architecturally and in molar mass) melt as in the present case.

For these calculations we assume that M_e and τ_e are independent of diene concentration and choose $M_e = 1120$ g/mol and $\tau_e = 1.1 \times 10^{-3}$ s at 155 ℃ corresponding to high density polyethylene.[52] With density 0.784g/cc, the chosen M_e is consistent with a plateau modulus of 1.99MPa. Phenomenologically both M_e and τ_e have been found to vary systematically with the comonomer content.[58,59] Also ring formation from diene has been implicated in variation of τ_e.[45] As our results in the previous section show, one can decrease the amount of incorporated diene by increasing the time of reaction (or residence time). Similarly, longer dienes can avoid ring formation due to the low probability of both the double-bonded ends being in close proximity of the growing chain end at the same time. We use the commonly used values for the dynamic dilation exponent α = 1 and the hopping parameter $p^2 = 1/40$.

We fix $x_f = 50$ for the semibatch case and $\tau_{res} = 100$ s for the CSTR case. For a given diene concentration, we generate 10^6 molecules. For computational efficiency in the rheology calculation we separate the molecules in 1000 bins equidistant in the logarithm of molar mass, retain a maximum of 10 molecules per bin and reassign the weights of the deleted molecules to the surviving molecules from the same bin. The resulting ensemble was used to calculate the rheological properties. Resampling from the same initial 10^6 molecules give very similar results. At each diene concentration, we repeat the whole procedure five times to estimate the statistical errors in our results.

Figure 13(a) and (b) respectively show the shear stress relaxation function $G(t)$ and the complex viscosity $\eta^*(\omega)$ for the semibatch case. The lines indicate power-law behavior fitted in the time range $10 - 100$s for $G(t)$ and frequency range $0.01 - 0.1$ rad/s for $\eta^*(\omega)$. Either of

these plots can be used to estimate the exponent $u = 0.36(1)$. The corresponding plots for the CSTR case in **Figure 14**(a) and (b) gives the exponent $u = 0.48(1)$. By fitting the zero shear viscosity η_0 and the recoverable compliance J_e^0 in power-law forms as a function of distance to the gelpoint ε, we find the viscosity exponent $s = 4.53(7)$ and the recoverable compliance exponent $t = 3.45(5)$ for the semibatch case (Figure 13c and d), and $s = 1.19(8)$ and $t = 2.0(1)$ for the CSTR case (Figure 14 c and d). These fits used the data in the $0.2 \leq \varepsilon \leq 0.6$ range.

Even for the lowest value of ε considered here, $G(t)$ shows a power-law decay only in a limited range of time. The exponent u is similar for either reactor reflecting the hierarchical relaxation of entangled polymers. However, the zero-shear viscosity and the steady state compliance are dominated by stress decay at long times from the relaxation of the largest and most branched molecules. The differences in the high molar mass tail between the resins from the two reactors show up as significantly different exponents for η_0 and J_e^0 between the semibatch and the CSTR case. The divergence of η_0 for the CSTR case is much slower (with and exponent $s = 1.2$) than the semibatch case ($s = 4.5$). The exponent for the semibatch case is consistent with gelation of well-entangled polymers with several entanglements between branch-points.[42] The viscosity exponent for the CSTR case is similar to the Rouse model prediction[42] $s \approx 1.33$ despite the inter-branch point segments being significantly longer than one entanglement. We can reconcile this by noting that due to the presence of trace amount of highly branched molecules the long-time relaxation of the CSTR resins is dominated by constraint release Rouse motion,[60,61] having the same dynamical form as of un-entangled Rouse beads.

5. Discussions

In this work, we considered the copolymerization of a bi-functional monomer (ethylene) and a tetra-functional comonomer (non-conjugated diene) using a metallocene catalyst in either a CSTR or a semibatch reactor. Gelation can be achieved in either of the reactors by increasing

the concentration of diene. We used a Monte Carlo scheme to sample representative molecules and calculate the molecular weight distributions. This method avoids closure approximations used in commonly used moments-based calculations. Unlike most theoretical treatments of gelation,[1,2,7,8,39] consideration of realistic reactor conditions leads to a distribution of reaction probabilities. In spite of this distribution in the reaction probabilities, the approach to gelation in the semibatch reactor is characterized by diverging weight averaged molar mass with the static exponents identical to the simple theoretical picture that considers a constant reaction probability. The same conclusion was previously reached for the approach to gelation in a free-radical polymerization scheme in a batch reactor.[10] For a diffusion limited lattice model of free-radical polymerization, the divergence of the weight averaged molar mass was found to hold,[9] albeit with an exponent that differs from polycondensation reactions.

In contrast, the results for the CSTR case fails to fit in this traditional picture: the weight averaged molar mass remains finite at gelation with the first moment to diverge being the fourth moment of the molar mass. The molar mass distribution close to gelation is characterized by a power-law tail with a non-universal exponent that depends on the details of the simulation parameters. Qualitatively, this heavy tail distribution results from a cooperative effect of the residence time of a particular segment and the probability of crosslinking: a segment residing for longer than average times in the reactor has higher probability of crosslinking and the segments to which it crosslinks themselves reside for longer than average times in the reactor. While our calculations only considered a particular class of chain-growth polymerization, such cooperative effect should be active in all chain polymerization schemes in CSTR where some crosslinking reaction step exists (for example, chain transfer to polymer together with termination by combination in free radical polymerization).

The heavy tailed nature of the molar mass distribution in CSTR for ethylene-diene copolymerization has implicitly been recognized in some theoretical calculations[32] and

experiments[31] by noting that the polydispersity index remains finite as the gel point is approached. However, the possibility that the weight averaged molar mass remain finite across the transition has been overlooked because of the approximate nature of the calculations. Since commonly measured low-ordered molar mass moments remain finite at gelation, predicting the gel-point from experimental data for this system should be difficult.

Experimentally polymer molar mass distribution is traditionally represented as the *weight* distribution normalized on the $log_{10}(M)$ axis. In **Figure 15**, we show the molar mass distributions for two values of ε for both the CSTR and the semibatch reactor cases in log-log scale (main plot) and log-linear scale (inset). In the traditional log-linear scale plot, we have omitted the data where $\frac{dw}{d\ log_{10}M} < 10^{-3}$, the typical sensitivity of the concentration detector in routine gel permeation chromatography (GPC) measurements. The plots for ε = 0.79 for both the CSTR and the semibatch cases are very similar. The ε = 0.07 curves are representative of the distributions as gelation is approached. In the semibatch case, a broad distribution with a high molecular weight tail can be easily seen in the linear-log plot; here the approach to gelation is obvious. In contrast, for the CSTR case at ε = 0.07, the linear-log representation appears to have only a marginally broader distribution as compared to ε = 0.79. Such broadening could easily be masked in industrial scale reactors by the much larger broadening arising from any non-ideality in the reactor conditions (such as temperature or concentration variations across the reactor) or other sources of experimental uncertainty. The gelation is only evident when viewing the log-log representation of the data, at levels far below the typical sensitivity of the concentration detector. We conclude that the CSTR case produces gelation whose onset is practically difficult, and perhaps impossible, to observe via conventional measurements.

Our calculations have focused here on idealized reactors (steady state CSTR and semibatch) and it is likely that additional complications will ensue in practical reactors. For example, it could take a very long time for a CSTR to achieve the steady state at which such large

molecules, as predicted by our algorithm, are actually generated.[12] Once generated, there is a possibility that strong flow fields in the reactor may break the molecules apart.[62,63] Nonetheless, the practical point of this paper, that gelation can occur significantly in advance of practical detection, remains.

Appendix

Incorporation of macromonomers

For the CSTR reactor, the concentration of macromonomers, $[P^{=}]$ is invariant in time and is given by

$$[P^{=}]_{CSTR} = \frac{k_{=}[Y]}{k_{PLCB}[Y] + s}. \tag{14}$$

Here, s is the flow rate defined as inverse of the mean residence time τ_{res}. For the semibatch reactor, $[P^{=}]$ depends on the current conversion x and is given by

$$[P^{=}]_{SB} = \frac{k_{=}}{k_{PLCB}} \left\{1 - exp\left(-\frac{k_{PLCB}}{k_p} x\right)\right\}. \tag{15}$$

Starting from a randomly selected monomer on a segment, in both the reactor types, the mean length to a branch-point from macromonomer incorporation is estimated by comparing the monomer incorporation rate to the macromonomer incorporation rate:

$$\bar{l}_m = \frac{k_p[M]}{k_{PLCB}\,[P^{=}]}. \tag{16}$$

For a segment growing at time t_c in a CSTR reactor, t_m, the time of creation of the incorporated macromonomer is estimated by considering the survival probability of macromonomers created at times prior to t_c and is given by the cumulative distribution function (CDF)

$$CDF(t_m) = exp\{-(k_{PLCB}[Y] + s)(t_c - t_m)\}. \tag{17}$$

Similarly, for a segment growing at conversion x_c in a semibatch reactor, the conversion x_m at which an incorporated macromonomer was created is given by

$$CDF(x_m) = \frac{exp\left(\frac{k_{PLCB}}{k_p} x_m\right) - 1}{exp\left(\frac{k_{PLCB}}{k_p} x_c\right) - 1}. \tag{18}$$

Incorporation of unreacted diene

Solely concentrating on the incorporated diene that eventually is incorporated in another growing chain at a later time before the end of the reaction, the mean-length to a branch-point of type b_{D1} for a chain growing at time t_c in the CSTR reaction is

$$\bar{l}_{D1} = \frac{k_p[M]}{k_{PD}\,[D]\{1 - exp(k_{DLCB}[Y]t_c)\}}. \tag{19}$$

The time at which this pendant once reacted diene is incorporated in another chain is given from

$$CDF(t_{D1}) = \frac{1 - exp\big(k_{DLCB}[Y]\ (t_c - t_{D1})\big)}{1 - exp(k_{DLCB}[Y]\ t_c)}. \tag{20}$$

For the semibatch reactor, concentration of available free diene depends on the conversion. Concentrating on a segment growing at conversion x_c, mean length to a branch-point of type b_{D1} is given by

$$\bar{l}_{D1} = \frac{k_p[M]}{k_{pD}\,[D]_0} \frac{exp\left(\frac{k_{pD}}{k_p} x_c\right)}{1 - exp\left(-\frac{k_{DLCB}}{k_p}(x_f - x_c)\right)}. \tag{21}$$

Here, the exponential term in the numerator accounts for varying diene concentration with conversion, and the denominator accounts for the fraction of incorporated free diene that had the chance to be reincorporated before the final conversion x_f. The conversion x_{D1} for this second incorporation event is given by

$$CDF(x_{D1}) = \frac{1 - exp\left(-\frac{k_{DLCB}}{k_p}(x_{D1} - x_c)\right)}{1 - exp\left(-\frac{k_{DLCB}}{k_p}(x_f - x_c)\right)}. \quad (22)$$

Incorporation of pendant diene

The steady state concentration of a once reacted diene in the CSTR reactor is given by

$$[D_1]_{CSTR} = \frac{k_{pD}[D][Y]}{k_{DLCB}[Y] + s}. \quad (23)$$

The mean length to a branch-point created by incorporation of a once reacted diene ($\bar{l}_{D2}$) is given by comparing the polymerization rate to the incorporation rate of D_1

$$\bar{l}_{D2} = \frac{k_p[M]}{k_{DLCB}\,[D_1]}. \quad (24)$$

Considering a once reacted diene incorporation at a time t_c, the chain on which this diene was first incorporated was created in the past at t_{D2} that follows

$$CDF(t_{D2}) = exp\{-(k_{DLCB}[Y] + s)(t_c - t_{D2})\}. \quad (25)$$

In the semibatch reactor, the mean length to a branch-point created by incorporation of once reacted diene depends on the conversion x_c at which a chain is growing and is given by

$$\bar{l}_{D2} = \frac{[M]}{[D]_0}\left(\frac{k_p}{k_{pD}} - \frac{k_p}{k_{DLCB}}\right)\left(exp\left(-\frac{k_{pD}}{k_p}x_c\right) - exp\left(-\frac{k_{DLCB}}{k_p}x_c\right)\right)^{-1}. \quad (26)$$

The conversion x_{D2} at which this incorporated D_1 had reacted for the first time is given by

$$CDF(x_{D2}) = \frac{1 - exp\left(-\left(\frac{k_{pD}}{k_p} - \frac{k_{DLCB}}{k_p}\right)x_{D2}\right)}{1 - exp\left(-\left(\frac{k_{pD}}{k_p} - \frac{k_{DLCB}}{k_p}\right)x_c\right)}. \quad (27)$$

Reincorporation after termination

A fraction $\frac{k_=}{k_= + k_s}$ of growing chains terminates with a double bond in either of the reactors. For a chain growing at time t_c in a CSTR and terminating with a double bond, a fraction $\{1 - \exp(k_{PLCB}[Y]t_c)\}$ is reincorporated before the chain exits from the reactor ($t = 0$). The time of this reincorporation is decided from

$$CDF(t_r) = \frac{1 - exp\big(k_{PLCB}[Y]\ (t_c - t_r)\big)}{1 - exp(k_{PLCB}[Y]\ t_c)}. \tag{28}$$

For the semibatch reaction with a chain ending with a double bond at a conversion x_c, a fraction $\left\{1 - exp\left(-\frac{k_{PLCB}}{k_p}\left(x_f - x_c\right)\right)\right\}$ of chains ending with a double bond is reincorporated before the final conversion x_f. The conversion for such a reincorporation is given by

$$CDF(x_r) = \frac{1 - exp\left(-\frac{k_{PLCB}}{k_p}\ (x_r - x_c)\right)}{1 - exp\left(-\frac{k_{PLCB}}{k_p}\ \left(x_f - x_c\right)\right)}. \tag{29}$$

Recursive construction of molecules

For both reactors, we start by randomly selecting a reacted monomer (that is attached to some polymer molecule) as it exits the reactor in the CSTR case (arbitrarily chosen origin of time, $t = 0$), or, at the end of the reaction in the semibatch case ($x = x_f$). From the exponential residence time in the CSTR,[13] the time t_c at which the selected monomer reacted is given by

$$CDF(t_c) = \exp(s\ t_c). \tag{30}$$

We assign this t_c by generating a random number uniformly between zero and one and setting the CDF equal to this random number. Analytical inversions are possible for all the CDF expressions derived here. When considering the conversion x as the time variable for semibatch reactor, the selected monomer has uniform probability of reacting between $x = 0$ and $x = x_f$.

The two directions along the chain from the selected monomer are not equivalent because of the flow (in CSTR) or catalyst deactivation (in semibatch). Each segment has a unique end at which the termination event happens (the catalyst detaches). We denote this end the downstream end and the opposite end (at which the initiation starts) is designated as the upstream end. The average number of monomer in the downstream direction for either of the two reactors is given by considering the ratio of the monomer addition rate to that of the termination and is given by

$$\overline{N}_{down} = \frac{k_p[M]}{k_= + k_s}. \tag{31}$$

The average number of monomer in the upstream direction is calculated by considering the ratio of the monomer addition rate to that of initiation, and for the CSTR case, is given by

$$\overline{N}_{up} = \frac{k_p[M]}{k_= + k_s + s}, \tag{32}$$

and in the semibatch case by

$$\overline{N}_{up} = \frac{k_p[M]}{k_= + k_s - k_d}. \tag{33}$$

Because of the high reactivity of metallocene catalysts, the synthesis of a primary segment (from initiation to termination) can be considered as instantaneous. Since the monomers are added at the catalyst site at a constant rate, we generate Flory distributed random numbers from these average values and use them as the upstream and the downstream segment lengths from the randomly chosen monomer.

For the moment concentrating on the upstream direction, we calculate the mean distance to a branch-point created from the macromonomer insertion, $\overline{l}_m$ from Equation 16; mean length to a branch-point formed by incorporating a free diene that reacted for the second time at a later stage of the reaction, $\overline{l}_{D1}$ from Equation 19 for CSTR (or from Equation 21 for semibatch); and

the mean distance to a branch-point formed by incorporating a pendant diene that was part of another chain, $\bar{l}_{D2}$ from Equation 24 for CSTR (or from Equation 26 for semibatch) case. The mean distance to a branch-point created from any of these three possibilities is given by

$$\bar{l}_B = \left(\frac{1}{\bar{l}_m} + \frac{1}{\bar{l}_{D1}} + \frac{1}{\bar{l}_{D2}} \right)^{-1}. \tag{34}$$

The distance to the next branch-point is determined by generating a Flory distributed random number with average given by $\bar{l}_B$. If this distance is less than the current segment length, a branch-point is considered at that distance. The branch-point is due to macromonomer insertion with probability

$$Prob(m) = \frac{\bar{l}_B}{\bar{l}_m}, \tag{35}$$

and a similar method is applied for calculating the probabilities of the branch-point being due to incorporation of a free diene or due to incorporation of a pendant diene attached to another chain segment.

Once we have decided on a branch-point, we move our focus recursively to the incorporated branch. If the branch-point is due to macromonomer incorporation, we only need to consider the upstream direction (since macromonomers are grafted at the terminal double bond). We assign the time of synthesis of the grafted macromonomer for the CSTR from Equation 17 or the conversion of the macromonomer from Equation 18. As with the initial segment, we associate a length with this segment and decide if branches should be added.

If the branch is created through incorporating a free diene that subsequently got incorporated in another growing chain, we assign the time (or conversion for semibatch reactor) from Equation 20 (or from Equation 22) to the chain that incorporated the diene for the second time. For the newly added segment, we need to consider both the upstream and the downstream directions. For a branch-point created by incorporating a pendant diene, the calculation is similar.

However, the time is now is determined from Equation 25 for the CSTR or the conversion from Equation 27.

Moving back to our original segment, we repeat our attempt to find the next branch point along the upstream direction from the current branch point. If the next branch point is predicted to lie beyond the end of the current segment, we conclude there are no more branch points and the search for branch points ends.

Starting from the first selected monomer, we follow the same steps along the downstream direction in creating branches. When the next branch-point in the downstream direction is predicted to be outside the segment, we decide if the segment terminated with a double bond and if so, if it was reincorporated in another growing chain at a later time (or conversion) following the probability expressions in the subsection titled "Reincorporation after termination". If the chain is decided to have been reincorporated, new segments are grown from the terminal monomer in both the upstream and downstream directions with time given from Equation 28 for the CSTR (or conversion from Equation 29 for semibatch reactor).

Since our attention is always on one segment considered to have grown instantaneously, the algorithm sketched above can be coded in a simple recursive form. Since we start with a randomly selected monomer, the algorithm selects molecules in a weight-biased ensemble, with each of the generated molecules carrying the same weight fraction.

Received: Month XX, XXXX; Revised: Month XX, XXXX; Published online:

DOI: 10.1002/mats.((insert number))

Keywords: (Sol-Gel transition, ethylene-diene polymerization, Monte Carlo Simulation, Computational rheology, long-tailed distribution)

[1] P. J. Flory, *J. Am. Chem. Soc.* **1941**, 63, 3083.

[2] W. H. Stockmayer, *J. Chem. Phys.* **1943**, 11, 45.

[3] P. J. Flory, *Principles of polymer chemistry*, Cornell University Press, Ithaca, N. Y., USA **1953**.

[4] M. Rubinstein, R. H. Colby, *Polymer Physics*, Oxford University press, Oxford, **2003**.

[5] E. M. Valles, C. W. Macosko, *Macromolecules* **1979**, 12, 673.

[6] D. Durand, M. Delsanti, M. Adam, J. M. Luck, *Eur. Phys. Lett.* **1987**, 3, 297.

[7] M. Gordon, *Proc. R. Soc.* A **1962**, 268, 240.

[8] C. W. Macosko, D. R. Miller, *Macromolecules* **1976**, 9, 199.

[9] H. J. Herrmann, D. P. Landau, D. Stauffer, *Phys. Rev. Lett.* **1982**, 49, 412.

[10] H. Tobita, A. E. Hamielec, *Macromolecules* **1989,** 22, 3098.

[11] H. Tobita, *J. Poly. Sc. Poly. Phys.* **1993**, 31, 1363.

[12] H. Tobita, *e-Polymers* **2004**, 4, 878.

[13] O. Levenspiel, *Chemical reaction engineering*, 3rd ed., Wiley, New York, **1999**.

[14] D. Yan, W.-J. Wang, S. Zhu, *Polymer* **1999**, 40, 1737.

[15] A. D. Gotsis, B. L. F. Zeevenhoven, A. H. Hogt, *Polymer Eng. Sc.* **2004**, 44, 973.

[16] D. J. Read, D. Auhl, C. Das, J. den Doelder, M. Kapnistos, I. Vittorias, T. C. B. McLeish, *Science* **2011**, 333, 1871.

[17] H. Braunschweig, F. M. Breitling, *Coordination Chemistry Revie*ws **2006**, 250, 2691.

[18] J. B. P. Soares, A. E. Hamielec, *Macromol. Theory Simul.* **1996**, 5, 547.

[19] P. J. Flory*, J. Am. Chem. Soc.* **1947**, 69, 2893.

[20] E. K. Gladding, B. S. Fisher, J. W. Collette, *I & E Chem. Prod. Res. Dev.* **1962**, 1, 65.

[21] K. R. Geddes, US Patent 4957982, **1990**.

[22] T. E. Nowlin, F. Y. Lo, R. S. Shinomoto, P. P. Shirodkar, US Patent 5332706, **1994**.

[23] A. H. Willbourn, *J. Poly. Sc.* **1959**, 34, 569.

[24] C. T. Elston, US patent 3984610, **1976**.

[25] P. Meka, K. Imanishi, G. F. Licciardi, A. C. Gadkari, US Patent 5670595, **1997**.

[26] A. K. Mehta, C. S. Speed, J. A. M. Canich, N. Baron, B. J. Folie, M. Sugawara, A. Watanabe, H. C. Welborn, US Patent 6300451 B1, **2001**.

[27] P. Agarwal, W. Weng, A. Mehta, A. Dekmezian, M. Chang, R Chudgar, C. Davey, C. Lin, M. Chen, G. Richeson, US Patent 20020013440 A1, **2002**.

[28] R. P. Duttweiler, M. J. Krause, F. Y. K. Lo, S. M. C. Ong, P. P. Shirodkar, US patent 6509431, 2003.

[29] P. Pietikäinen, J. V. Seppälä, L. Ahjopalo, L.-O. Pietilä, *Eur. Poly. J.* **2000**, 36, 183.

[30] E. Kokko, P. Pietikäinen, J. Koivunen, J. V. Seppälä, *J. Poly. Sc. Poly. Chem.* **2001**, 39, 3805.

[31] J. D. Gunzmán, D. J. Arriola, T. Karjala, J. Gaubert, B. W. S. Kolthammer, *AIChE J*. **2010**, 56, 1325.

[32] G. ver Strate, C. Cozewith, W. W. Graessley, *J. Appl. Polymer Sc*. **1980**, 25, 59.

[33] M. Nele, J. B. P. Soares, J. C. Pinto, *Macromol. Theory Simul.* **2003**, 12, 582.

[34] R. Li, A. B. Corripio, K. M. Dooley, M. A. Henson, M. J. Kurtz, *Chem. Eng. Sc*. **2004**, 59, 2297.

[35] R. C. S. Dias, M. R. P. F. N. Costa, *Macromol. React. Eng*. **2007**, 1, 440.

[36] P. D. Iedema, M. Wulkow, C. J. Hoefsloot, *Macromolecules* **2000**, 33, 7173.

[37] D. Beigzadeh, J. B. P. Soares, T. A. Duever, A. E. Hamilec, *Poly. React. Eng.* **1999**, 7, 195.

[38] H. Tobita, Macromol. *React. Eng*. **2013**, 7, 181.

[39] D. Stauffer, *J. Chem. Soc. Faraday Trans. 2* **1976**, 72, 1354.

[40] D. Stauffer, A. Coniglio, M. Adam, *Adv. Polym. Sc*. **1982**, 44, 103.

[41] P. G. de Gennes, *J. Physique Lett*. **1977**, 38, 355.

[42] C. P. Lusignan, T. H. Mourey, J. C. Wilson, R. H. Colby, *Phys. Rev. E* **1999**, 60, 5657.

[43] C. Das, N. J. Inkson, D. J. Read, M. A. Kelmanson, T. C. B. McLeish, *J. Rheol*. **2006**, 50, 207.

[44] M. Doi, S. F. Edwards, *The theory of polymer dynamics*, Clarendon Press, Oxford, **1986**.

[45] C. Das, D. J. Read, J. M. Soulages, P. P. Shirodkar, *Macromolecules* **2014**, 47, 586.

[46] N. J. Inkson, C. Das, D. J. Read, *Macromolecules* **2006**, 39, 4920.

[47] D. J. Read, T. C. B. McLeish, *Macromolecules* **2001**, 34, 1928.

[48] W. H. Press, S. A. Teukolsky, W. T. Vetterling, B. P. Flannery, *Numerical recipes in C++: The art of scientific computing*, 2nd ed., Cambridge University Press, **1992**.

[49] H. Tobita, *Macromolecules* **2004**, 37, 585.

[50] C. Das, D. J. Read, M. A. Kelmanson, T. C. B. McLeish, *Phys. Rev. E* **2006**, 74, 011404.

[51] bob2.5. http://sourceforge.net/projects/bob-rheology, **2012**.

[52] C. Das, D. J. Read, D. Auhl, M. Kapnistos, J. den Doelder, I. Vittorias, T. C. B. McLeish, *J. Rheol*. **2014**, 58, 737.

[53] P. G. de Gennes, *J. Chem. Phys*. **1971**, 55, 572.

[54] T. C. B. McLeish, *Europhys. Lett*. **1988**, 6, 511.

[55] R. G. Larson, *Macromolecules* **2001**, 34, 4556.

[56] G. Marrucci, *J. Polym. Sci., Polym. Phys. Ed*. **1985**, 23, 159.

[57] E. van Ruymbeke, C. Bailly, R. Keunings, D. Vlassopoulos, *Macromolecules* **2006**, 39, 6248.

[58] L. J. Fetters, D. J. Lohse, C. A. García-Franco, P. Brant, D. Richter, *Macromolecules* **2002**, 35, 10096.

[59] X. Chen, F. J. Stadler, H. Münstedt, R. G. Larson, *J. Rheol*. **2010**, 54, 393.

[60] J. Klein, *Nature* **1978**, 271, 143.

[61] J. L. Viovy, M. Rubinstein, R. H. Colby, *Macromolecules* **1991**, 24, 3587.

[62] D.-M. Kim, M. Busch, H. C. J. Hoefsloot, P. D. Iedema, *Chem. Eng. Sc*. **2004**, 59, 699.

[63] N. Yaghini, P. D. Iedema, *Chem. Eng. Sc*. **2015**, 130, 310.

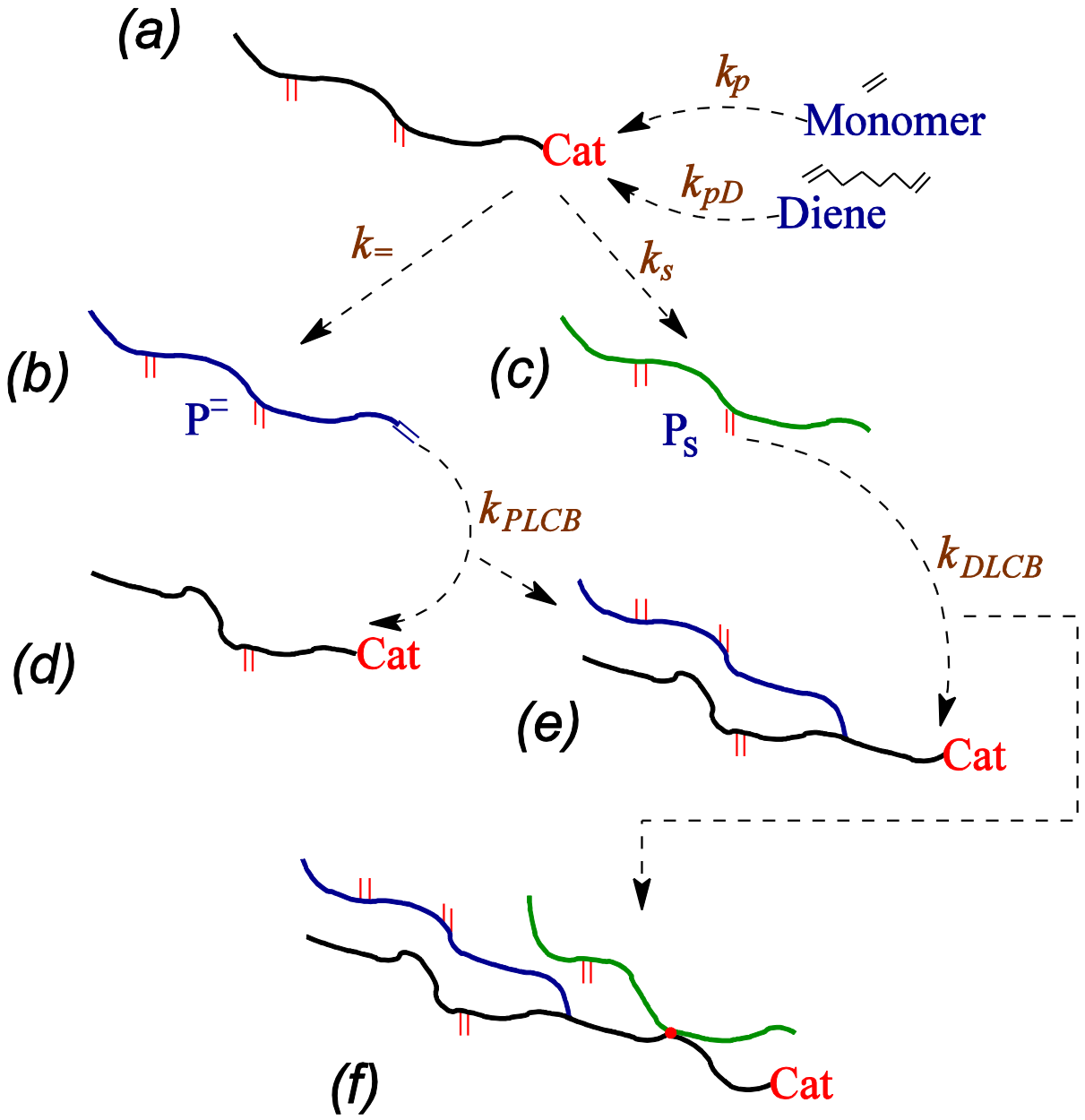

Figure 1. Schematic reaction scheme for ethylene-diene copolymerization with a metallocene catalyst: (a) propagation, (b) termination with a terminal double bond (macromonomer), (c) termination with a saturated chain end, (d) incorporation of macromonomer to generate three functional long-chain branches, and (e) incorporation of pendant diene to generate (f) four functional long-chain branches.

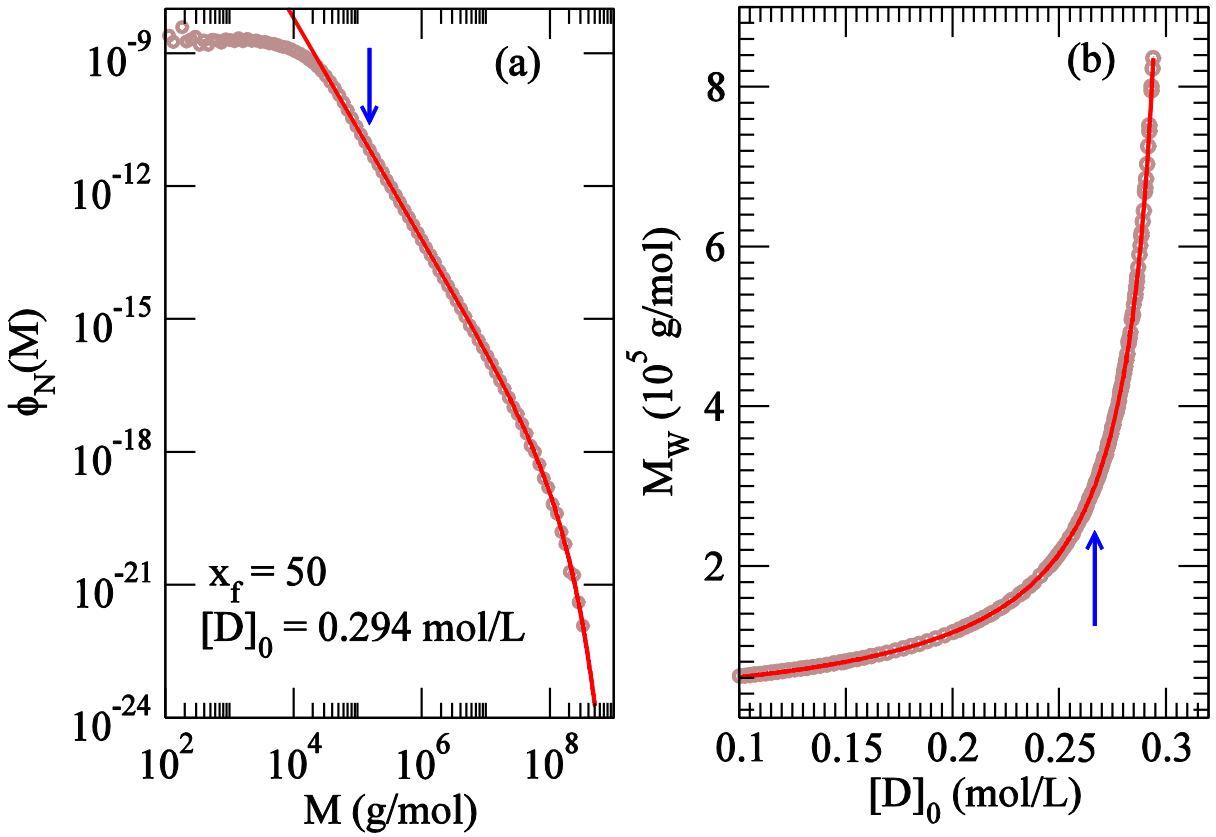

Figure 2. (a) Number distribution at $x_f = 50$ and $[D]_0 = 0.294$ mol/L. The fit line has the functional form $55.2 \exp\left(-\frac{M}{5.76\times10^7}\right) M^{-2.49}$ for which data above $M = 2 \times 10^5$ g/mol (indicated by the arrow) was used. (b) Weight averaged molar mass as a function of $[D]_0$ for $x_f = 50$. The line shows the fit $M_W = 41.2 \times 10^3 (1 - [D]_0/0.3095)^{-1.005}$. The data for $[D]_0 > 0.264$ mol/L (indicated by the arrow) was used for the fit.

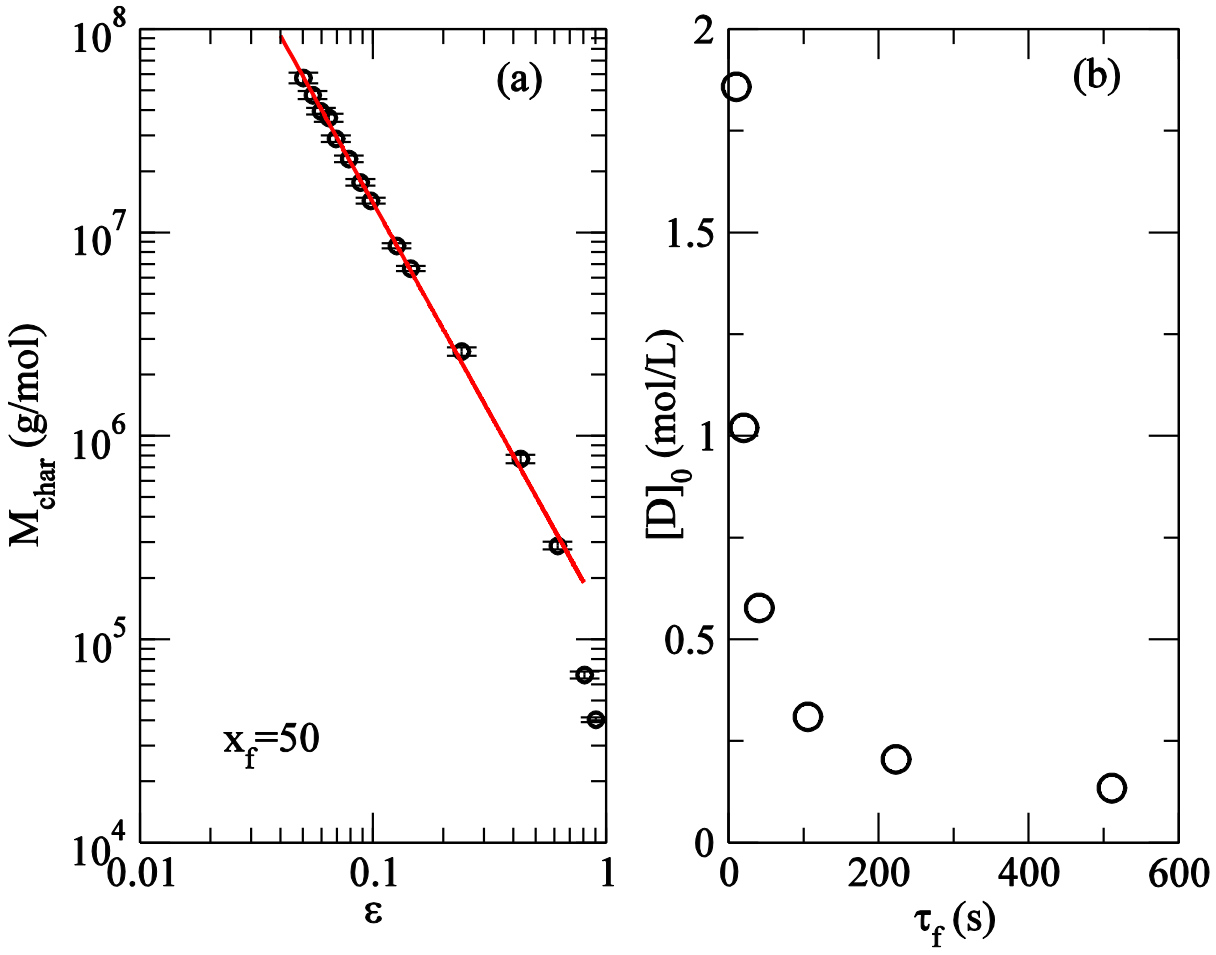

Figure 3. (a) M_{char} diverges as a power of ε. The line is a fit $M_{char} = 1.2 \times 10^5\ \varepsilon^{-2.06}$. The data for the largest two values of ε was excluded in the fitting. (b) Initial diene concentration required to reach gelation as a function of reaction time in the semibatch reactor.

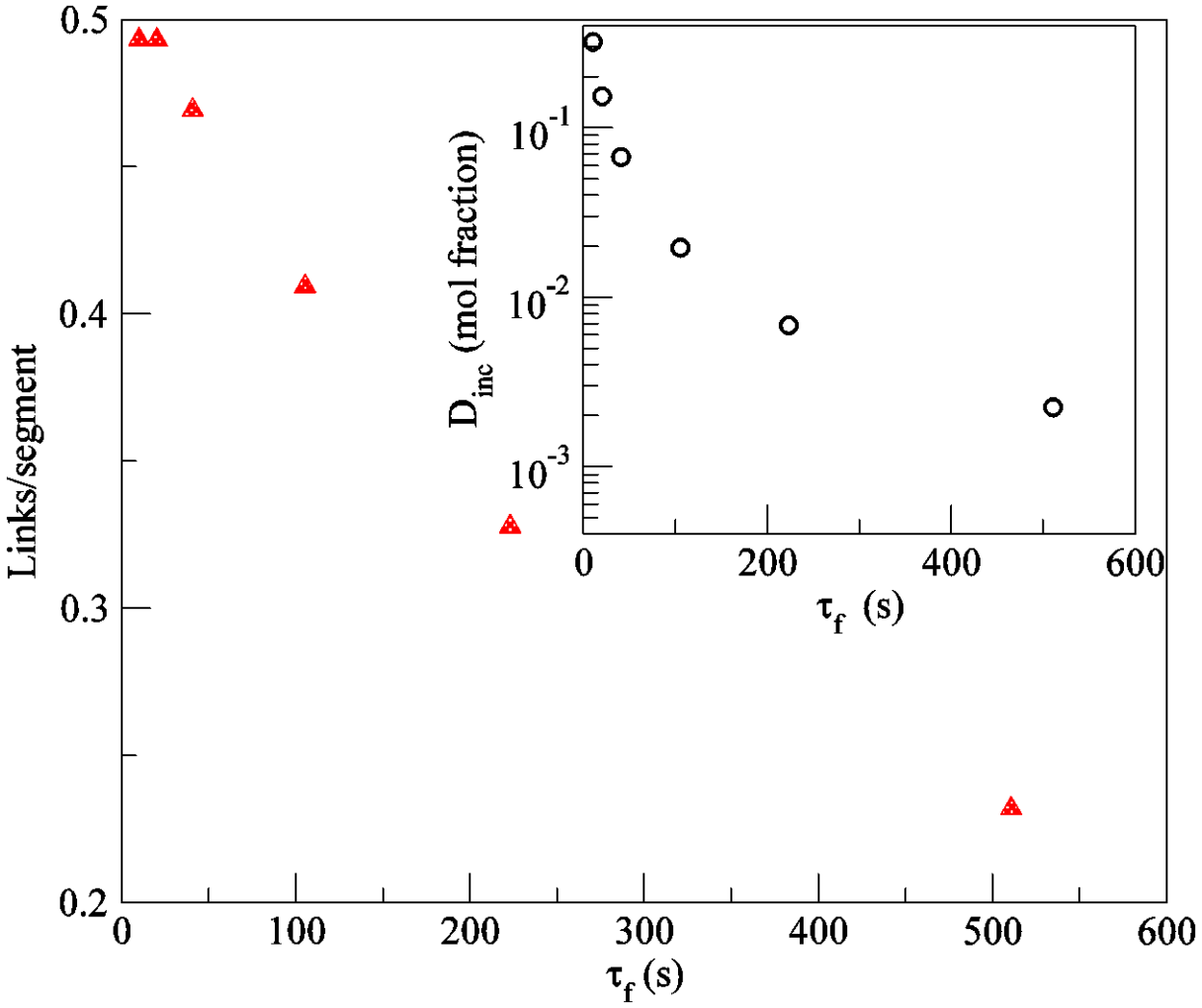

Figure 4. Diene links per primary segment at gelation (at the critical diene concentration) as a function of time of reaction. Inset: Mole fraction of incorporated diene as a function of reaction time.

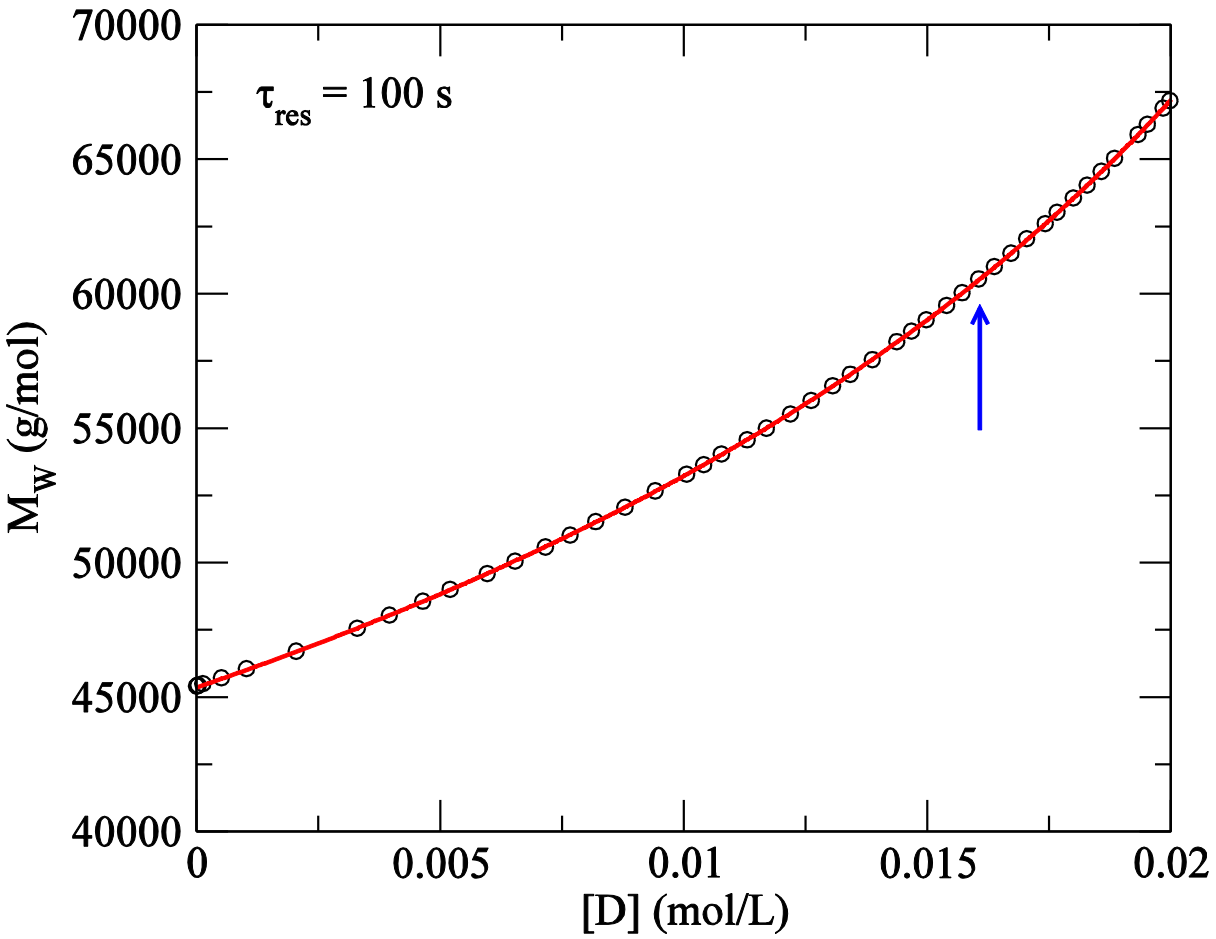

Figure 5. Weight averaged molar mass as a function of diene concentration in CSTR with residence time $\tau_{res} = 100$ s. The line is a power-law fit yielding $[D]_c = 0.0373(1)$ mol/L and exponent -0.513(2). For the fit, only the data above $[D] > 0.016$ mol/L (indicated by the arrow) was considered.

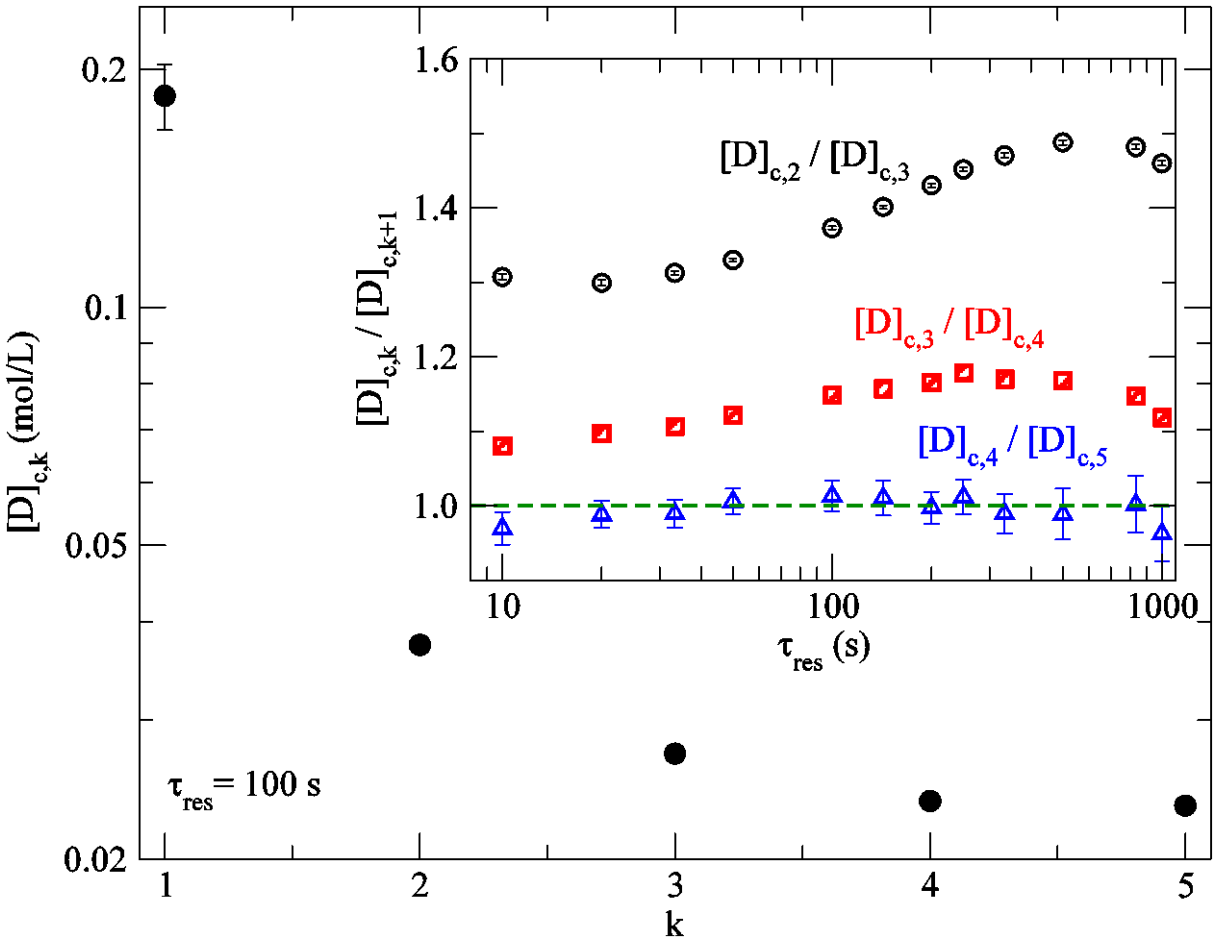

Figure 6. Critical diene concentration $[D]_{c,k}$ estimated from power-law fit of the k-th moment of the molar mass for resins generated in CSTR conditions with $\tau_{res} = 100$ s. Inset: Ratio of critical diene concentrations estimated from successive molar mass moments as a function of τ_{res}.

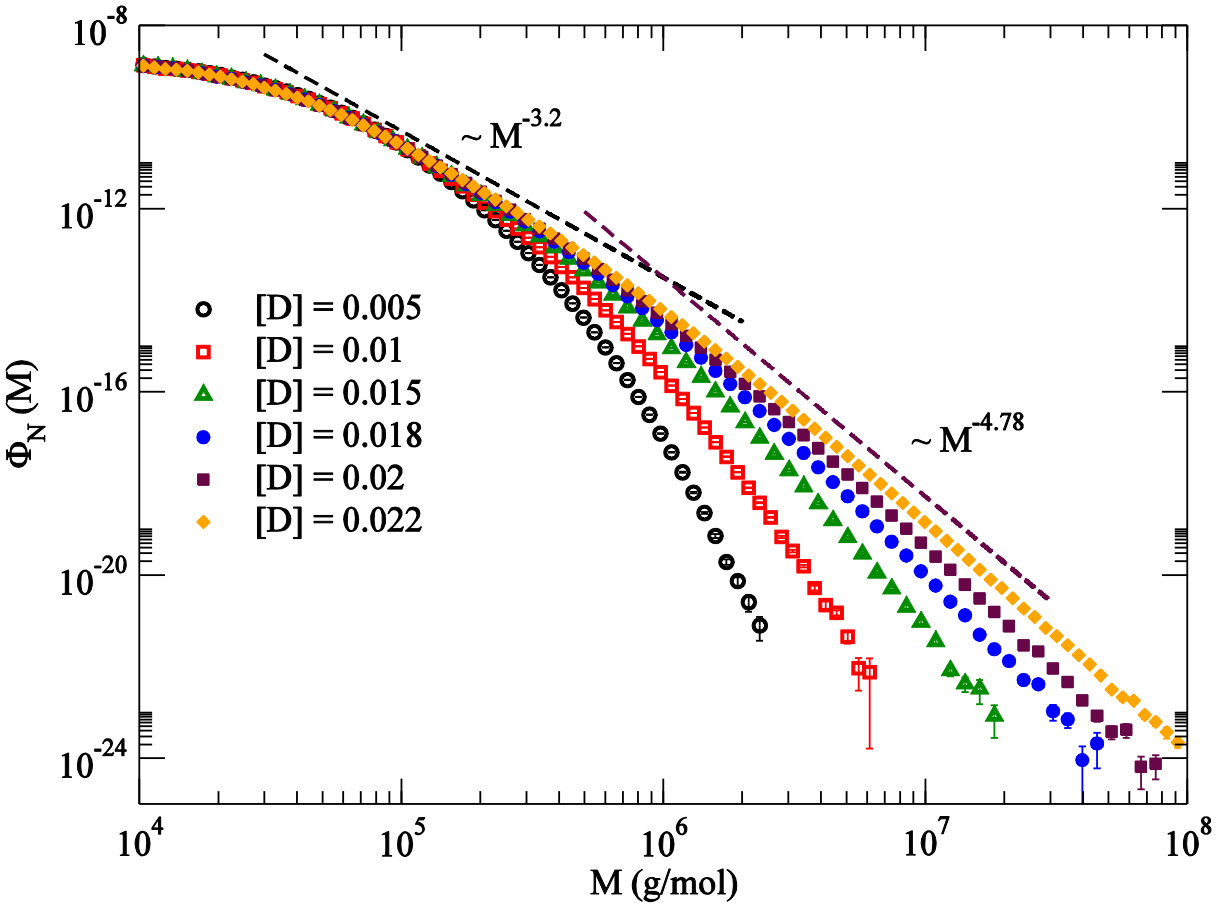

Figure 7. Number distributions for the indicated diene concentrations in CSTR with $\tau_{res} = 100$ s. For the highest diene concentration, we show two different local power-law trends that describes the data in the intermediate range (with power -3.2) and in the high molar mass tail (with power -4.78).

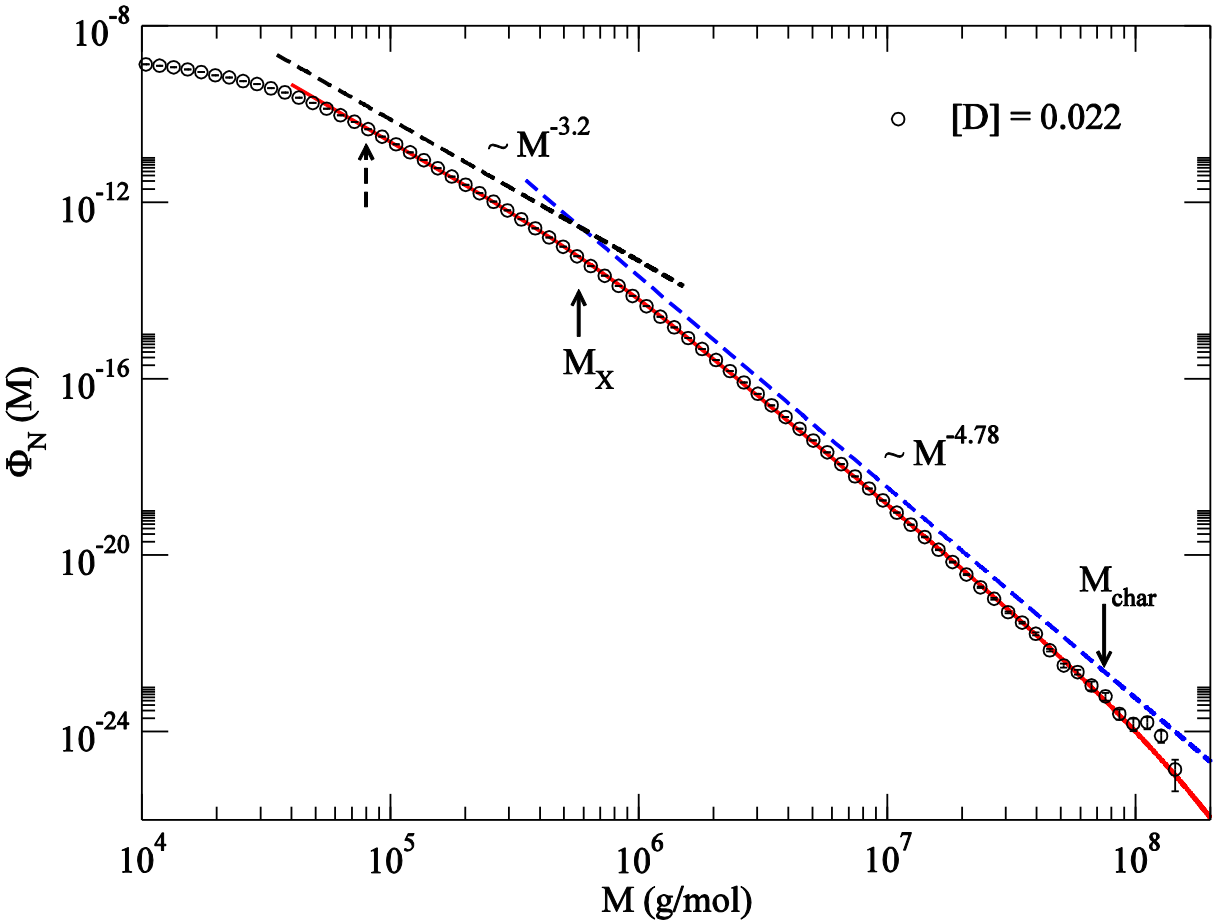

Figure 8. Number distribution (symbols) with $[D] = 0.022$ mol/L and $\tau_{res} = 100$ s in CSTR. The solid line is a fit of the form Equation 9 with $\tau_1 = 3.20(1)$, $\tau = 4.78(2)$, $M_X = 5.8(2) \times 10^5$ g/mol, and $M_{char} = 1.6(1) \times 10^8$ g/mol. Only data for molar mass greater than 8×10^4 g/mol (indicated by the dashed arrow) was used for the fit.

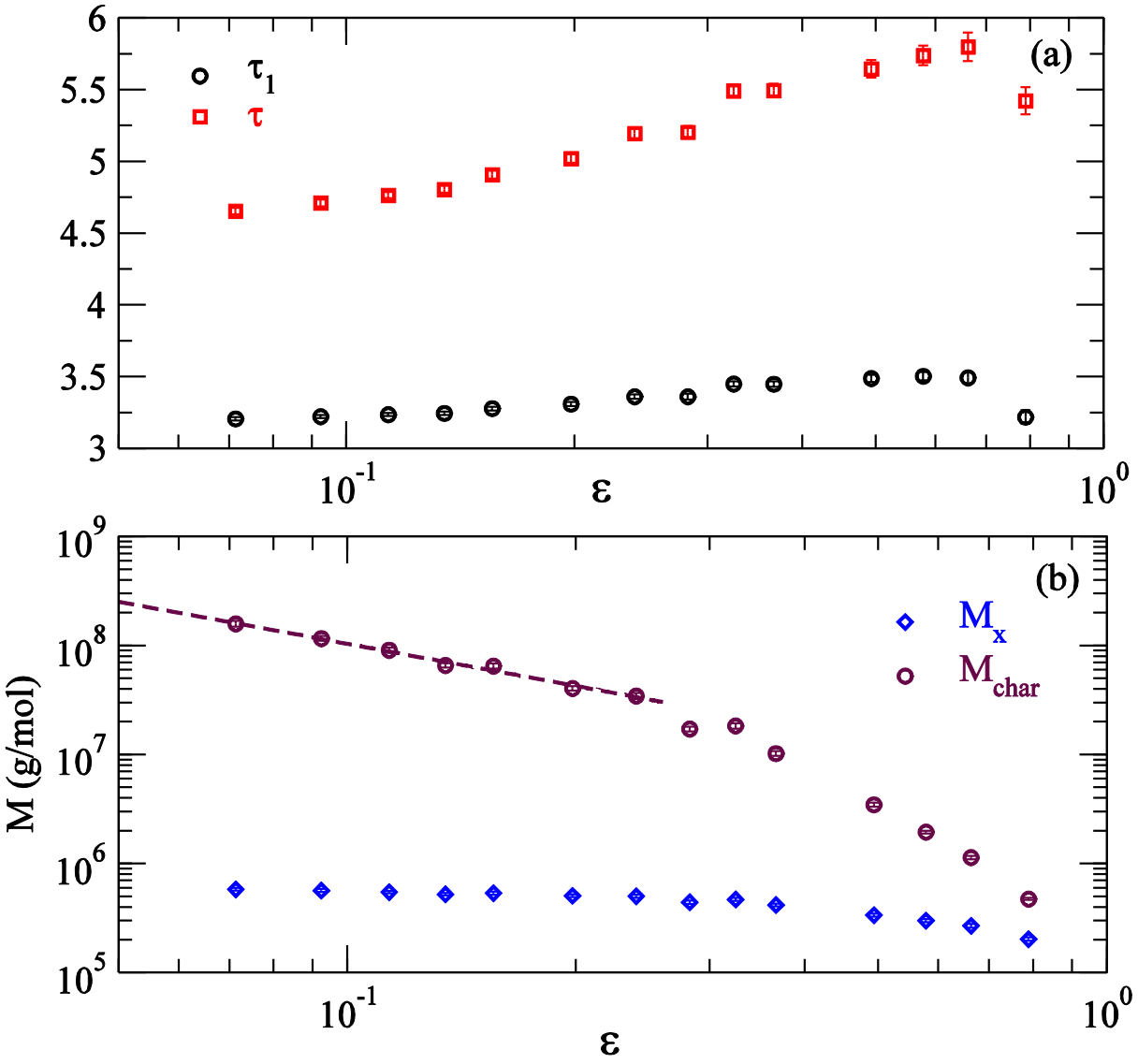

Figure 9. (a) Exponents that describe the number distribution in the intermediate molar mass (τ_1), and in the high molar mass (τ) regions as a function of closeness to the gel-point ε in CSTR with $\tau_{res} = 100$ s. (b) The cross-over molar mass between the two power-law regions M_X, and the characteristic molar mass M_{char} as a function of ε. The dashed line is a fit of the form $M_{char} = 5.4 \times 10^6 \, \varepsilon^{-1.28(6)}$ in the drawn region.

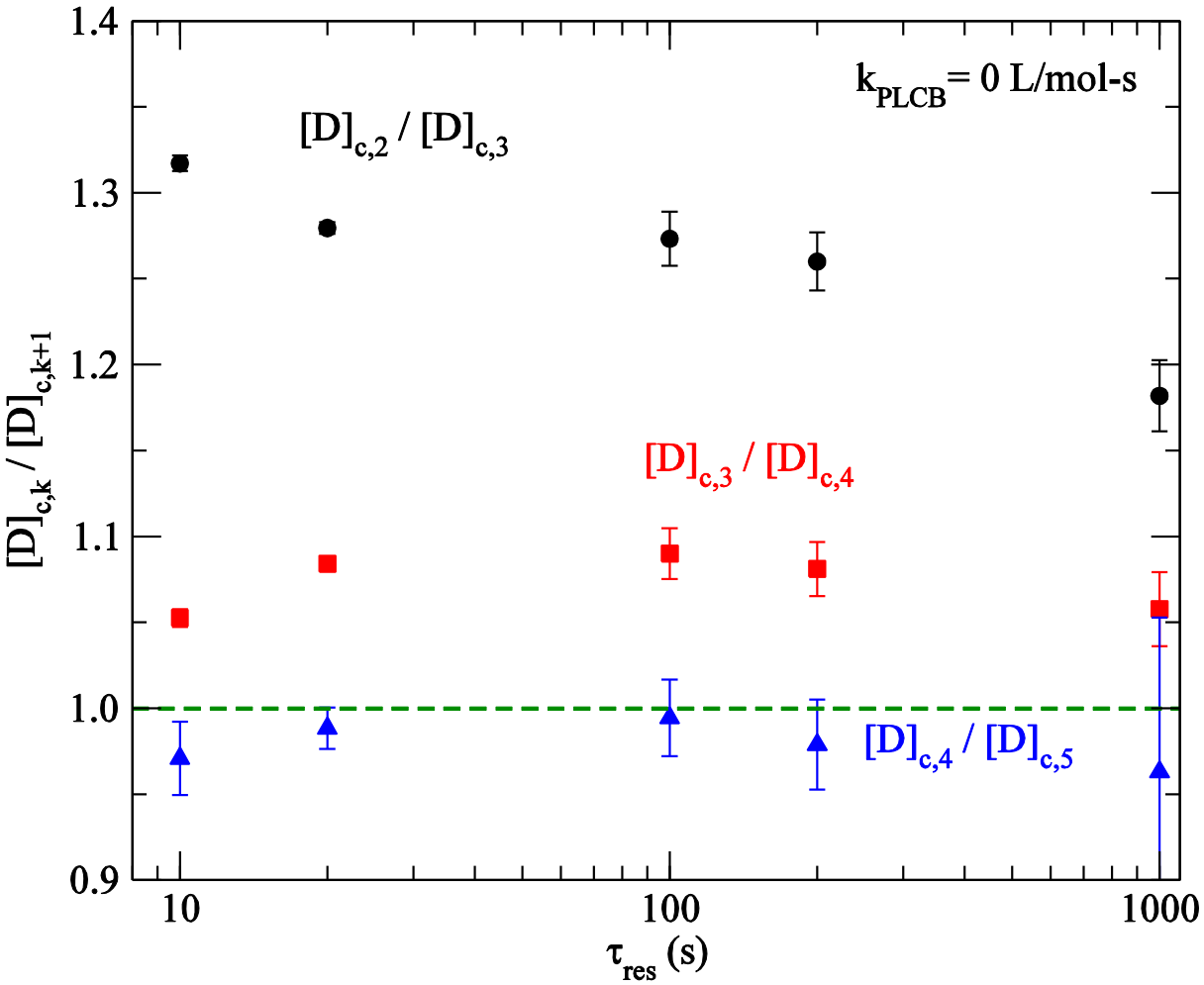

Figure 10. Ratio of diene concentrations at which successive moments of molar mass is extrapolated to diverge as a function of τ_{res} for the case where macromonomer incorporation is not allowed.

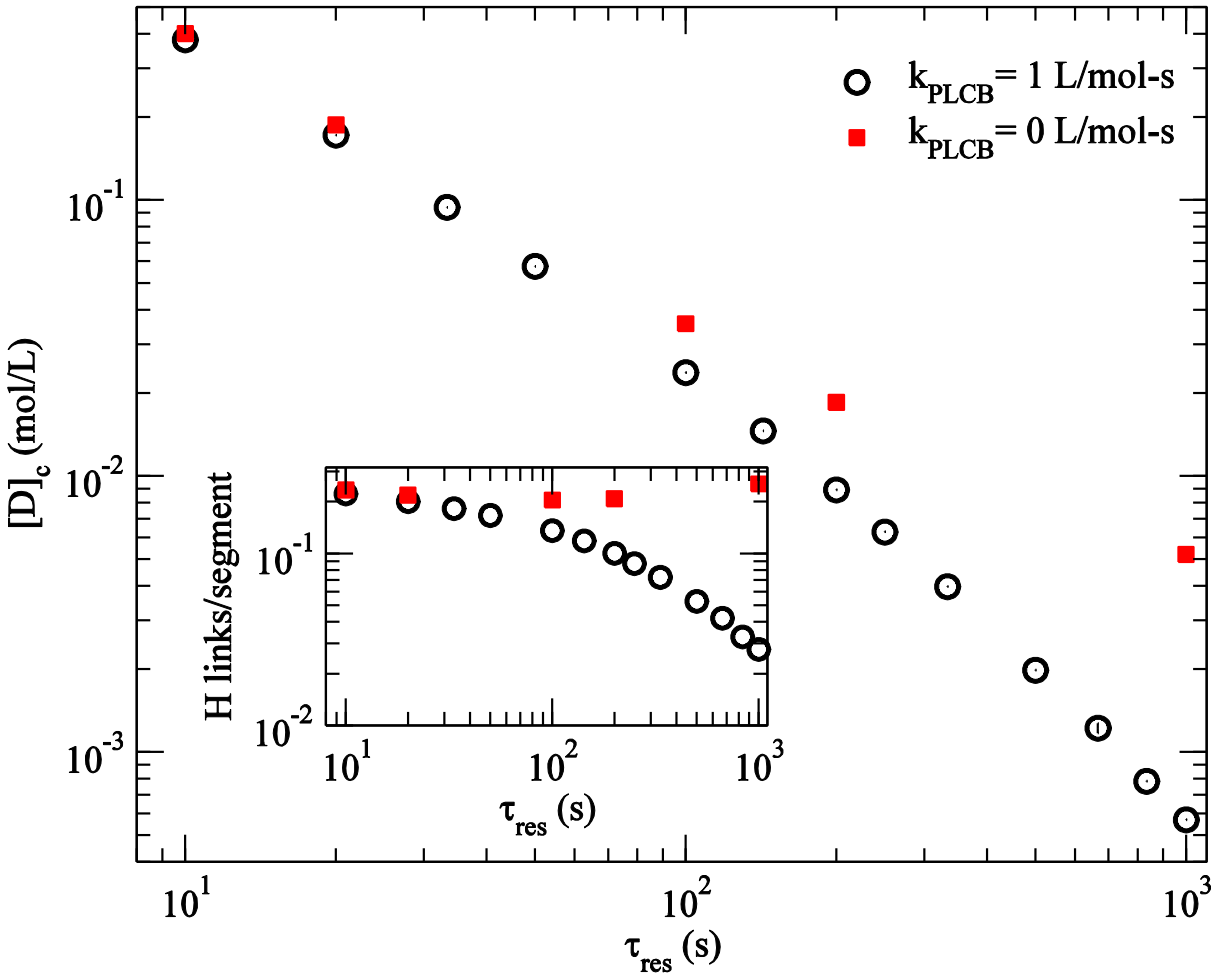

Figure 11. Critical diene concentration as a function of residence time: Open circles and filled squares correspond to the case with macromonomer incorporation (with k_{PLCB} = 1 L/mol-s) and to the case where macromonomer incorporation is prohibited, respectively. Inset: Estimated number of diene links per (weight averaged) segment at gelation.

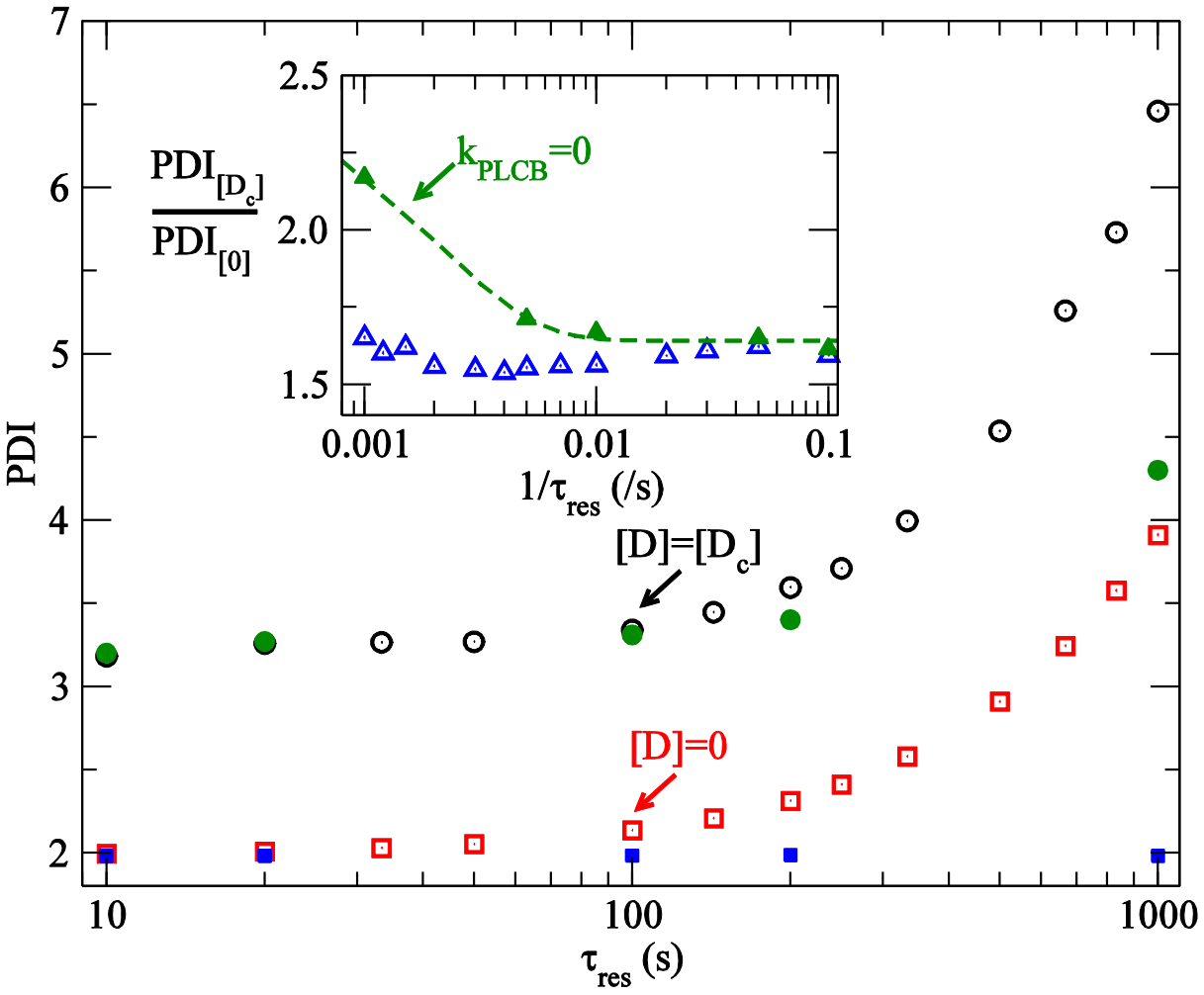

Figure 12. Polydispersity index as a function of τ_{res}. Square symbols are PDI without diene, circles are extrapolated values at critical diene concentrations corresponding to the relevant τ_{res}. Open symbols are from simulations with $k_{PLCB} = 1$ L/mol-s, closed symbols are from simulations with $k_{PLCB} = 0$. Inset: Ratio of PDI at critical diene concentration to diene-free reactions. Open and closed symbols respectively refer to the case with and without macromonomer incorporation. The dashed line is a fit for $k_{PLCB} = 0$ data of the form $1.64 + 0.86 \exp(-490\ \tau_{res})$.

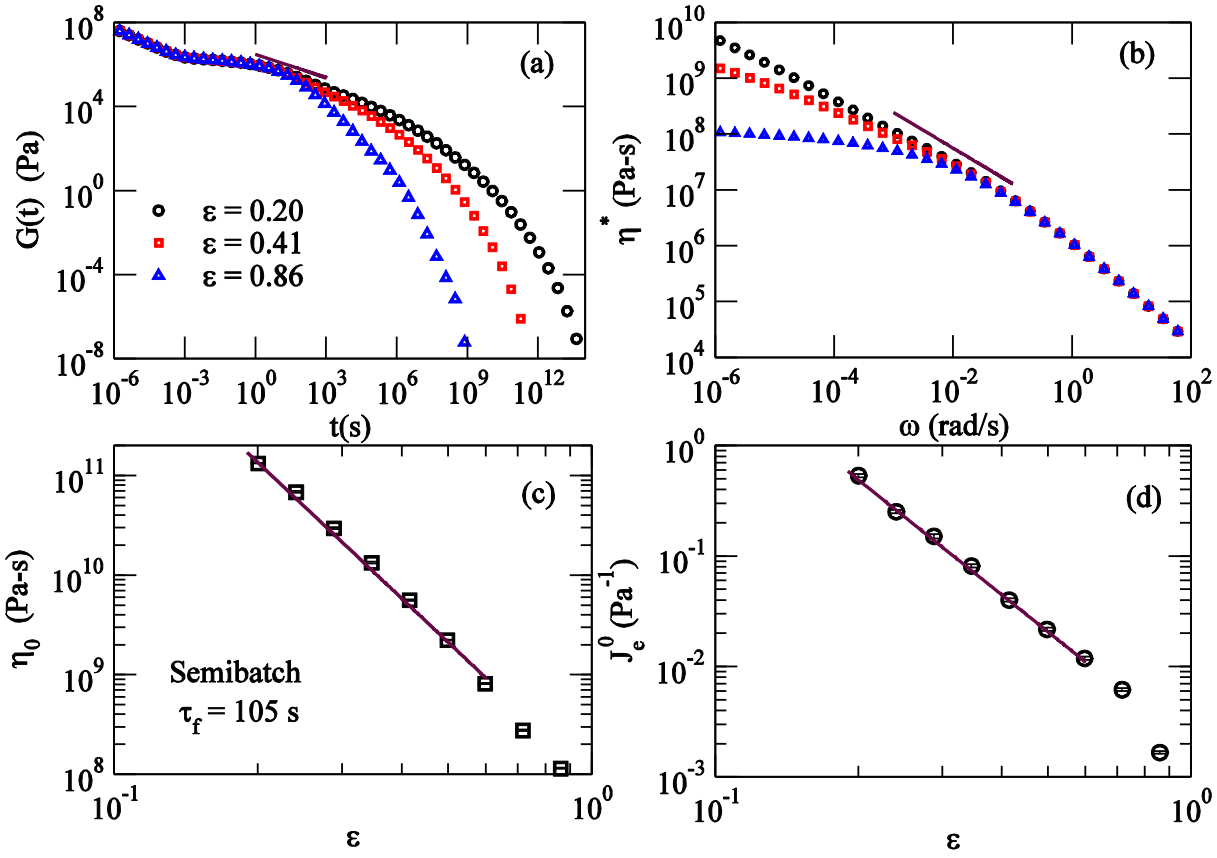

Figure 13. Dynamic scaling for relaxation in the melt for semibatch reactor: (a) Shear stress relaxation function and (b) dynamic viscosity show power-law behaviours in time and frequency respectively. (c) The zero shear viscosity and (d) the recoverable compliance diverges as a power of closeness to the gel point.

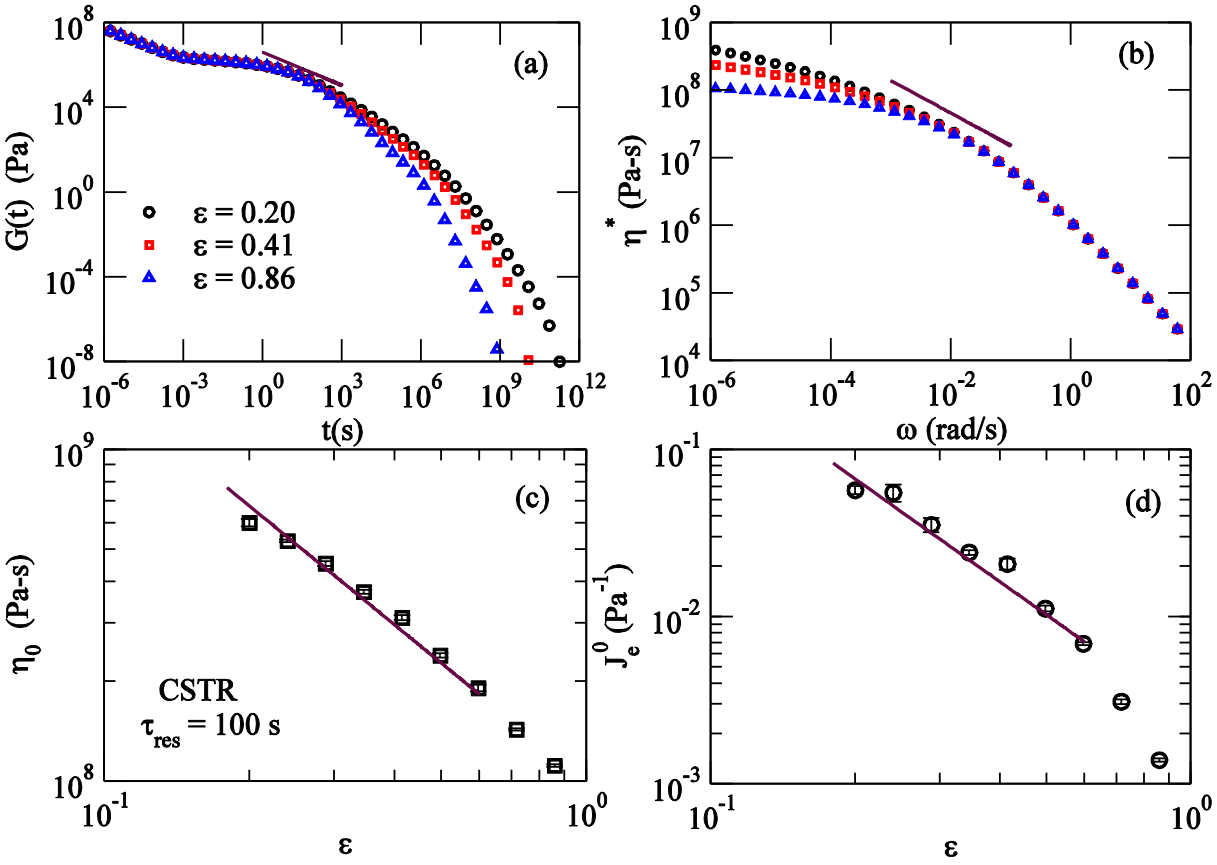

Figure 14. Dynamic scaling for relaxation in the melt for the CSTR case: (a) Shear stress relaxation function and (b) dynamic viscosity show power-law behaviours in time and frequency respectively. (c) The zero shear viscosity and (d) the recoverable compliance diverges as a power of closeness to the gel point.

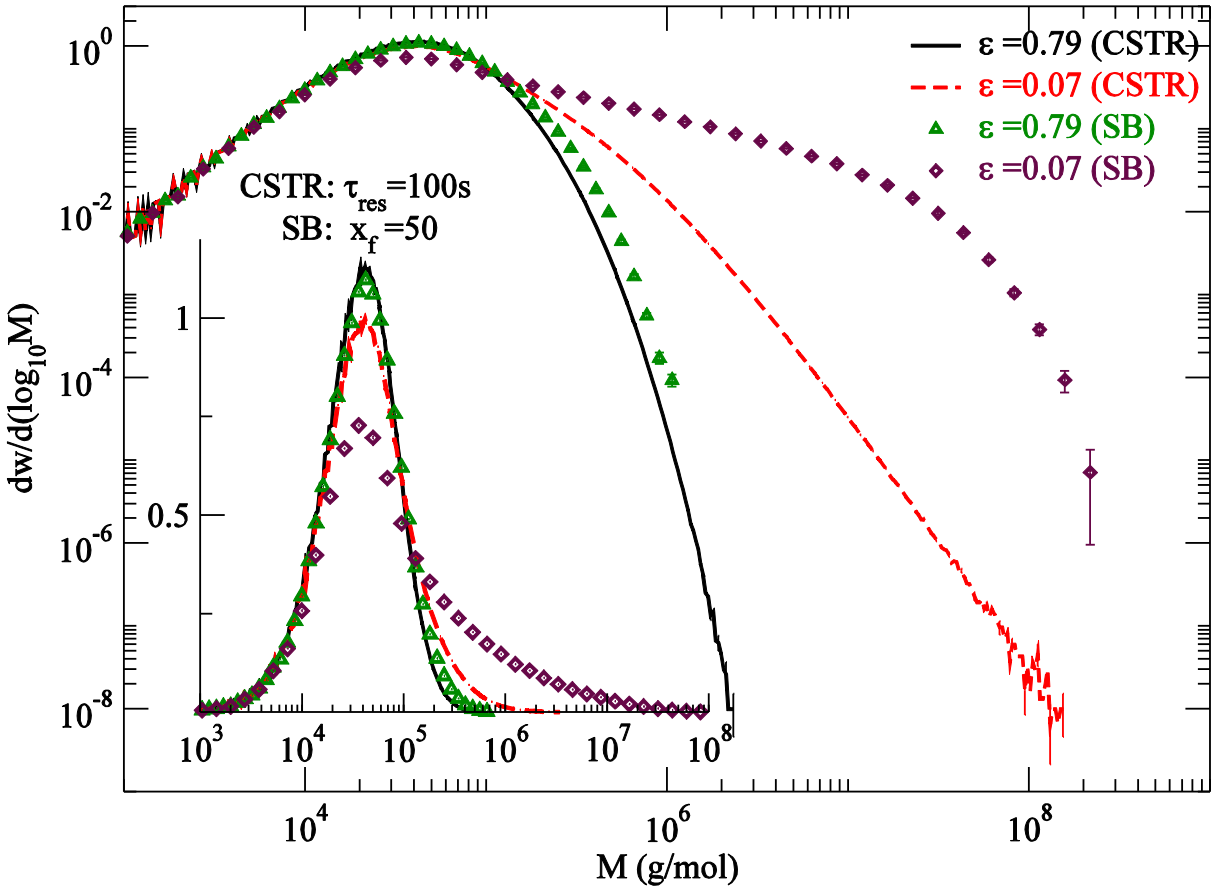

Figure 15. Molar mass distributions at fixed separations from gelation at ε=0.79 and ε=0.07 for CSTR (lines) and semibatch (symbols) reactors. Inset: Molar mass distribution in traditional linear-log scale.

Table of content entry

Copolymerization of two and four functional groups in semibatch reactor leads to diverging weight averaged molar mass and zero shear viscosity with an exponent -4.5 as gelation is approached with increasing amount of four functional groups. In contrast, in continuous stirred tank reactor, the number, weight and z-averaged molar masses remain finite and viscosity diverges with an exponent -1.2.

Chinmay Das*, Daniel J. Read*, Johannes M. Soulages, Pradeep P. Shirodkar

Static and dynamic scaling close to gelation in chain-polymerization: Effect of reactor type